Discovery of a potent dual SLK/STK10 inhibitor based on a maleimide scaffold

Ricardo A. M. Serafim[1,2], Fiona J. Sorrell[3], Benedict-Tilman Berger[4,5], Ross J. Collins[6], Stanley N. S. Vasconcelos[1,2], Katlin B. Massirer[1,2], Stefan Knapp[4,5], James Bennett[3], Oleg Fedorov[3], Hitesh Patel[6], William J. Zuercher[7,*] and Jonathan M. Elkins[2,3*]

[1] Center for Medicinal Chemistry (CQMED), Center for Molecular Biology and Genetic Engineering (CBMEG), University of Campinas (UNICAMP), Campinas, SP 13083-875, Brazil.

[2] Structural Genomics Consortium, University of Campinas (UNICAMP), Av. Dr. André Tosello, 550, Barão Geraldo, Campinas / SP 13083-886, Brazil.

[3] Centre for Medicines Discovery, University of Oxford, Old Road Campus Research Building, Old Road Campus, Roosevelt Drive, Oxford, OX3 7DQ, UK.

[4] Structural Genomics Consortium, Johann Wolfgang Goethe University, Buchmann Institute for Molecular Life Sciences, Max-von-Laue-Str. 15, D-60438 Frankfurt am Main, DE, Germany.

[5] Institute for Pharmaceutical Chemistry, Johann Wolfgang Goethe University, Max-von-Laue-Str. 9, D-60438 Frankfurt am Main, DE, Germany.

[6] Medicines Discovery Institute, School of Biosciences, Cardiff University, Cardiff, CF10 3AT, UK.

[7] Structural Genomics Consortium, UNC Eshelman School of Pharmacy, University of North Carolina at Chapel Hill, Chapel Hill, NC 27599, USA.

*Correspondence:
jon.elkins@cmd.ox.ac.uk
william.zuercher@unc.edu

Abstract

SLK (STE20-like kinase) and STK10 (serine/threonine kinase 10) are closely related kinases whose enzymatic activity is linked to the regulation of ezrin, radixin and moesin function and to the regulation of lymphocyte migration and the cell cycle. We identified a series of 3-anilino-4-arylmaleimides as dual inhibitors of SLK and STK10 with good kinome-wide selectivity. Optimization of this series led to multiple SLK/STK10 inhibitors with nanomolar potency. Crystal structures of exemplar inhibitors bound to SLK and STK10 demonstrated the binding mode of the inhibitors and rationalized their selectivity. Cellular target engagement assays demonstrated binding of the inhibitors to SLK and STK10 in cells. Further selectivity analyses, including analysis of activity of the reported inhibitors against off-targets in cells, identified compound **31** as the most potent and selective inhibitor of SLK and STK10 yet reported.

Introduction

SLK (STE20 like kinase) and STK10 (serine/threonine kinase 10, also known as LOK) are serine/threonine kinases whose major known function is activating the ERM (ezrin/radixin/moesin) proteins by phosphorylation on a conserved threonine residue near the C-terminus (moesin Thr558)[1,2]. This phosphorylation relieves an auto-inhibited state of the ERM proteins allowing them to bind to the plasma membrane via their N-terminal FERM domain and to F-actin via their C-terminal region[3–5].

SLK and STK10 are both enriched in cellular membrane protrusions called microvilli, and are important in the regulation of localizing microvilli to the apical aspect of epithelial cells[6]. This localization control is linked to the phosphorylation of ezrin by SLK and STK10 which serves to promote ezrin localization at the apical aspect; as well as being the major ERM kinases in lymphocytes, SLK and STK10 are also the major ERM kinases in epithelial cells, and delocalized STK10 kinase activity caused delocalization of ezrin[6]. Based on the experiments with the *Drosophila* paralogue Slik, SLK and/or STK10 may be important for epithelial integrity[2].

Both SLK and STK10 consist of an N-terminal kinase domain of the STE20 subfamily and a large C-terminal domain consisting of coiled-coil regions that mediate protein:protein interactions[7–9]. SLK and STK10 also have roles, as yet poorly defined, in regulating the cell cycle and apoptosis: both kinases are able to phosphorylate polo-like kinase 1 (PLK1)[10–13]. During lymphocyte apoptosis, ERM phosphorylation by STK10 is prevented by caspase cleavage of STK10 which separates the N-terminal kinase domain and the C-terminal regulatory domain[14]. Both N- and C-terminal domains of STK10 are required for ERM phosphorylation due to a complex mechanism in which the C-terminal domain primes ERM proteins for phosphorylation by the kinase domain[15]. SLK is also cleaved by a caspase, caspase 3, enabling cytoskeletal changes and again resulting in apoptosis[8,16]. The N-terminal kinase domain of SLK is known to be activated by an activation loop exchange mechanism in which the kinase domains dimerize to allow auto-phosphorylation[17], and SLK dimerization was shown to increase SLK activity on substrates relevant for the pro-apoptotic role of SLK[18].

Potent and specific small molecule inhibitors allow detailed studies of the roles of proteins in biology and disease, including ascertaining the likely effects of pharmacological targeting. SLK and STK10 have similar ATP-binding sites with only one amino acid difference on the edge of the binding pocket. Due to this high similarity, to obtain specific inhibitors for SLK or STK10 will likely require a thorough understanding of the structure-activity relationships and selectivity across different inhibitor chemotypes, together with structural data on the available conformations of the kinase domain.

The chemogenomic sets PKIS and PKIS2 contain biologically and chemically diverse kinase inhibitors with potent activity on approximately one third of the protein kinome[19,20]. PKIS2 was profiled as a single measurement at 1 μM in the DiscoverX KINOMEscan panel of approximately 400 wild type human kinase assays. Compounds having a selectivity profile of S(35) < 0.04 were progressed for K_D measurement with

those kinases binding >80%. Previously we published the discovery and characterization of an imidazole series of dual STK10/SLK inhibitors with higher inhibitory potential for STK10 than SLK[19]. Here we present the identification, optimization and characterization of a series of potent dual SLK/STK10 inhibitors derived from a maleimide scaffold identified in the PKIS2 screening data. From this series we developed a potent, selective and cell penetrant dual SLK/STK10 inhibitor, the most potent and selective SLK/STK10 inhibitor yet developed.

Results

Identification of a maleimide starting point for SLK/STK10 inhibition

From a set of maleimide compounds that were tested at 1 µM in binding-displacement assays against around 400 protein kinases[20] we identified a set of maleimide compounds with potent SLK binding and selectivity over the majority of the kinome (Table 1). Dose-response measurements confirmed that 3-anilino-4-arylmaleimide (**1**) had K_D = 770 nM against SLK, K_D = 460 nM against CLK2, and K_D = 580 nM against GSK3A, while MKNK1 and PDPK1 were false positives in the original screen.

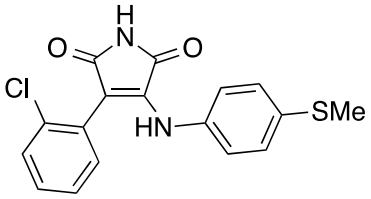

1

Kinase	%I @ 1 µM	K_D (nM)
MKNK1	100	>10000
SLK	**99**	**770**
CLK2	88	460
GSK3A	81	580
PDPK1	80	>10000
DYRK1B	78	ND
MEK6	76	ND
NEK1	75	ND
CLK1	74	ND
PKAC-alpha	74	ND
DYRK1A	67	ND

Table 1. Maleimide hit **1** identified in PKIS2 KINOMEscan profiling[20]. The percentage inhibition at a compound concentration of 1 µM and the dissociation constant from dose-response measurement are shown.

Encouraged by the confirmation of SLK inhibition by **1**, we further investigated the 3-anilino-4-arylmaleimide series. The KINOMEscan experiment had identified other, structurally related compounds with high SLK binding at 1 µM and varying degrees of selectivity with respect to other protein kinases. We selected **1** and seven additional compounds with SLK %I > 50 for evaluation in ligand binding displacement assays for SLK and STK10 (Table 2). The SLK K_i values spanned two orders of magnitude, from 8.5 nM for **2** to 740 nM for **7**. The most potent compounds had *ortho* substituents on the aryl ring, and the aniline ring was limited to *meta* and/or *para* substitution. In this *in vitro* assay, the series showed a moderate (five- to tenfold) preference for SLK over its close phylogenetic relative STK10.

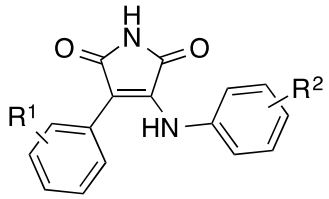

Cmpd	R[1]	R[2]	KINOMEscan @ 1 µM				Binding K_i (nM)		STK10/SLK
			S(35)	# of kinases		SLK %I			
				%I > 95%	%I > 80%		SLK	STK10	
1	2-Cl	4-SMe	0.03	2	4	99	59	760	13
2	2-OMe	3-Cl-4-OH	0.06	4	11	99	8.5	73	8.6
3	2-OMe	3-OH	0.05	6	12	99	60	480	8.0
4	2-Cl	3-Cl	0.04	9	11	96	28	310	11
5	3-OMe	3-Cl	0.04	3	9	92	120	950	7.9
6	3-OMe	4-SMe	0.01	0	0	78	400	3500	8.8
7	3-OMe	3-OH	0.04	8	13	69	740	4100	5.5
8	2-Cl	H	0.02	1	3	51	69	560	8.1

Table 2. Confirmation of SLK affinity of PKIS2 hits in ligand binding displacement assays. K_i values were determined in a binding displacement assay (n=2 technical replicates) and pIC_{50} values and associated errors can be found in Supplementary Table 1.

To verify the potential of the maleimide series to inhibit SLK in cells we performed a NanoBRET target engagement analysis. Two exemplar inhibitors were tested for their ability to displace a fluorescent tracer molecule (present at 2 µM) from a transiently expressed SLK-Nanoluc fusion protein in HEK293 cells. In this analysis, both **2** and **4** had an IC_{50} in HEK293 cells of ~1 µM (Supplementary Figure 1).

Chemistry

Having verified the potential of the maleimide scaffold for selective SLK/STK10 inhibition we proceeded with synthesis and evaluation of further maleimide derivatives. Initially, the synthesis was accomplished using a two-step synthetic route (Scheme 1). First, commercially available 2-substituted phenylacetamides were exposed to dimethyl oxalate in the presence of potassium *tert*-butoxide as base at 0 °C to generate a cyclized 4-hydroxymaleimide intermediate. Second, the desired 4-anilinomaleimide product was obtained via reaction of the 4-hydroxymaleimide with anilines or benzylamines through heating at 100 °C in acetic acid.

Scheme 1. Synthesis of maleimides **9**-**65**.

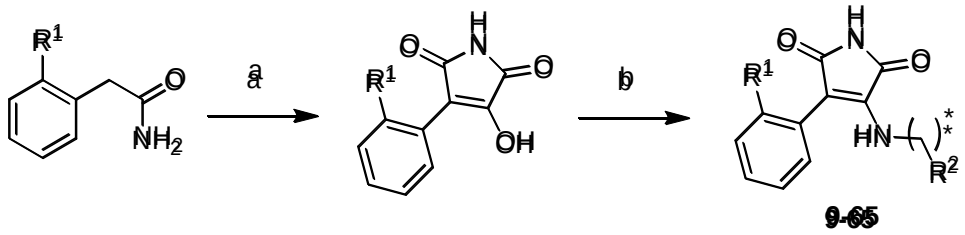

Reagents and conditions: a) dimethyl oxalate, *t*-BuOK, 0 °C to rt, 4 h; b) aniline or benzylamine* derivative, AcOH, 100 °C, 12 h. For identity of R_1 and R_2, see Tables 3, 4 and 7.

To introduce new substituents to the aryl ring of the maleimide scaffold, palladium-catalyzed coupling reactions (Suzuki-Miyaura and Buchwald-Hartwig) were performed to introduce new C-C and C-NH bonds. In pilot experiments, using different sources of palladium ($Pd(dppf)Cl_2$, $Pd(PPh_3)_4$, $Pd_2(dba)_3$, $Pd(OAc)_2$) and ligands (S-Phos, X-Phos, XantPhos, APhos, Me_3(OMetBuXPhos)) performing the coupling reaction on the 4-anilinomaleimide was unsuccessful. Therefore, the synthetic strategy was changed to perform the coupling reactions with the acetamide and methyl ester derivatives to create the C-C and NH-C bonds, respectively. The synthetic routes to introduce the aromatic/heteroaromatic rings and isobutyramide are shown in Scheme 2. Initially, activation of the carbonyl group of the carboxylic acid was performed by Fischer-Speier esterification followed by generation of acetamide by ammonium hydroxide in MeOH at 80 °C. The best condition for the Suzuki-Miyaura coupling was found to be $Pd(dppf)Cl_2$, Cs_2CO_3 and a 5:1 mixture of 1,4-dioxane/water at 85 °C to obtain the desired substituted acetamide intermediates. Subsequently, the reaction conditions in Scheme 1 were again used to obtain the 4-hydroxymaleimide intermediates, followed by introduction of the 3-cyano-aniline. A similar synthetic route was used to attach the isobutyramide group (Scheme 2), albeit in this case the Buchwald-Hartwig coupling was performed with the bromide derived from the isolated methyl ester using $Pd_2(dba)_3$, aided by the ligand XantPhos, Cs_2CO_3 and 1,4-dioxane as solvent at 85 °C. For the 4-phenoxy **43** and naphthyl **44** derivatives, the respective carboxylic acid starting materials were commercially available and were cyclized directly after obtaining their respective acetamides.

Scheme 2. Synthesis of maleimides substituted with aromatic/heretoaromatic rings, bromide or isobutyramide (**66**-**82**).

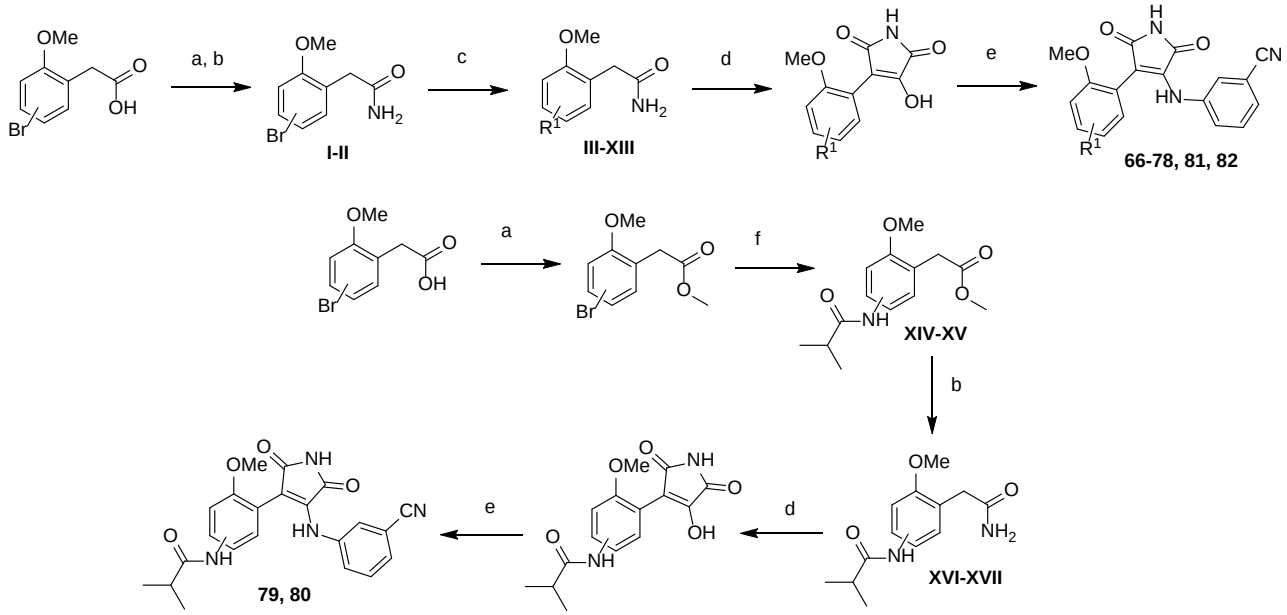

Reagents and conditions: a) MeOH, H_2SO_4 (cat), reflux, 10h; b) NH_4OH, MeOH, 80 °C, 10 h; c) Ar/Het-$B(OH)_2$, $Pd(dppf)Cl_2$, Cs_2CO_3, 1,4-dioxane:water (5:1), 85°C, 7 h; d) dimethyl oxalate, *t*-BuOK, 0 °C to rt, 4 h; e) 3-CN-aniline, AcOH, 100 °C, 12 h; f) isobutyramide, $Pd_2(dba)_3$, XantPhos, Cs_2CO_3, 1,4-dioxane, 85 °C, 8 h. For nature of R_1, see Table 8.

SAR exploration of the maleimide scaffold

In the initial SAR, a 2-OMe substituent was present in the most potent compounds. To expand on this SAR data, a set of maleimides was designed containing 2-substituted aryl groups (CF_3, Cl, and OMe) and a variety of substituents on the aniline ring. The resulting array of compounds was profiled in SLK and STK10 ligand binding displacement assays (Table 3). A general trend with the 2-aryl substituent was that 2-OMe compounds had the highest affinity, those with 2-CF_3 were the least potent, and compounds with 2-Cl substitution were intermediate in potency. The substitution on the aniline also affected potency with *meta/para* substituents on the aniline ring increasing the potency ~30-fold compared to *ortho* (e.g. **14**: K_i = 17 nM and **17**: K_i = 21 nM vs **11**: K_i = 490 nM). The *para* hydroxyl-substituted derivate **3** was marginally (~1.7x) more potent than the *meta* derivative **24**. The combination of a hydroxyl in *para* and a Cl atom in *meta* position of compound **2** was extremely potent (K_i = 8.5 nM) while compound **36** containing both *meta* positions substituted by Cl was much less potent (K_i = 110 nM). Removal of the *para*-hydroxyl, maintaining only one *meta*-Cl generated the slightly more potent compound **31** (K_i = 6.6 nM).

Since the *meta* position on the aniline ring was sensitive to different substitutions, electron-withdrawing groups were tested (-F, -CF_3 and -CN, compounds **27**, **29** and **41** respectively), yielding around a 2-fold

improved in potency with *meta*-CN on compound **41** (K_i = 3.7 nM). Modification with SO_2Me group did not increase potency (**18**, **19**). Compounds bearing a benzyl substituent rather than an aryl off the maleimide ring (**37-39**) displayed significantly reduced binding potency.

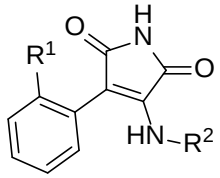

Cmpd	R_1	R_2	K_i (nM)		STK10/SLK
			SLK	STK10	
9	CF_3	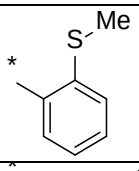	6900	26000	3.8
10	Cl		2900	12000	4.1
11	OMe		490	1300	2.7
12	CF_3	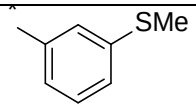	100	730	7.3
13	Cl		33	340	10.3
14	OMe		17	110	6.5
15	CF_3	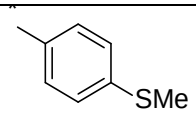	320	3200	10
16	Cl		62	680	11
17	OMe		21	140	6.7
18	Cl	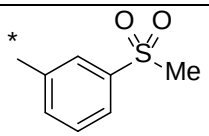	310	2300	7.4
19	OMe		95	630	6.6
20	CF_3	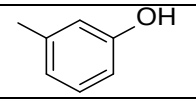	450	3400	7.6
21	Cl		56	560	10
22	CF_3	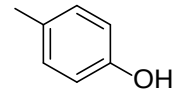	280	2200	7.9
23	Cl		40	300	7.5
24	OMe		35	200	5.7
25	CF_3	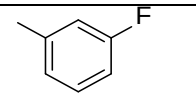	240	2100	8.8
26	Cl		44	380	8.6
27	OMe		13	76	5.8
28	Cl	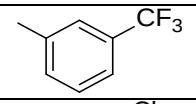	200	1500	7.5
29	OMe		61	340	5.6
30	CF_3	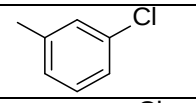	130	960	7.4
31	OMe		6.6	46	7.0
32	CF_3	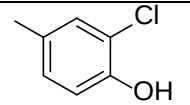	76	610	8.0
33	Cl		17	150	8.8
34	CF_3	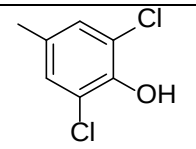	1600	9300	5.8
35	Cl		300	2300	7.7
36	OMe		110	590	5.4
37	CF_3		180000	130000	0.7
38	Cl		160000	190000	1.2

39	OMe	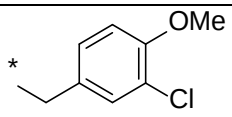	72000	450000	6.3
40	Cl	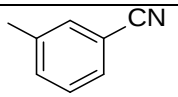	41	350	8.5
41	OMe		3.7	26	7.0
42	OPh		8400	33000	3.9
43	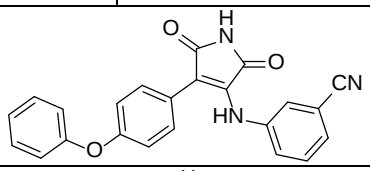		5400	NB	-
44	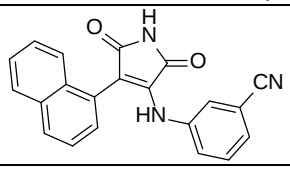		29	110	3.8

Table 3: K_i values were determined in a binding displacement assay. NB = no binding (>100 µM).

An additional six compounds with different patterns of OMe substitution on the aryl ring were also tested (**45-50**) but none of these structural modifications resulted in a potency improvement (Table 4).

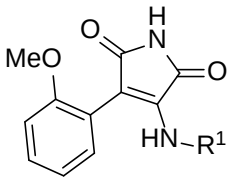

Compound	R_1	K_i (nM)		STK10/SLK
		SLK	STK10	
45	2-OMe-Ph	390	1500	3.8
46	3-OMe-Ph	29	180	6.2
47	4-OMe-Ph	22	120	5.5
48	2,4-$(OMe)_2$-Ph	500	2400	4.8
49	3,4-$(OMe)_2$-Ph	210	1100	5.2
50	3,5-$(OMe)_2$-Ph	86	480	5.6

Table 4. K_i values were determined in a binding displacement assay.

To confirm that the most potent compounds identified at this stage were genuine inhibitors of the enzymatic activity of SLK and STK10, compounds **31** and **41** were tested in an enzymatic assay (Table 5). Both compounds yielded IC_{50} values against SLK and STK10 in good agreement with the values from the binding displacement assay (Table 4). We also measured the IC_{50} values of **31** and **41** against CLK2, GSK3α and GSK3β as these were kinases identified as off-targets of the original maleimide compounds (Table 1), showing that while **31** and **41** showed about a 4-fold potency advantage for SLK and STK10 over CLK2, they were also potent inhibitors of GSK3α and GSK3β.

Kinase	IC_{50} (nM)			Control Cmpd
	31	**41**	**Control**	
SLK	7.8	8.2	19	Staurosporine
STK10	6.4	10	99	Ro-31-8220
CLK2	39	70	5.6	Staurosporine
GSK3α	14	19	5.1	Staurosporine
GSK3β	14	36	5.1	Staurosporine

Table 5. Enzymatic assay IC_{50} determination for compounds **31** and **41**. Assays were performed using a radiometric format (Reaction Biology Corp.).

The kinome selectivity of **31** and **41** was tested on a panel of ~400 wild-type protein kinases (Table 6) followed by testing of the top hits in a NanoBRET cellular assay, revealing that SLK was the top hit for both **31** and **41**. The selectivity of the compounds for SLK over STK10 seen in the binding-displacement assays was not seen in the enzymatic assay (Table 5) and only partially seen in the NanoBRET assay (Table 6). A good overall selectivity over the rest of the kinome was achieved with selectivity scores (S_{35}) of 0.040 and 0.062 for **31** and **41** respectively.

31			**41**		
Kinase	% of control (KINOMEscan)	Cellular IC_{50} (NanoBRET, μM)	Kinase	% of control (KINOMEscan)	Cellular IC_{50} (NanoBRET, μM)
JAK3@2	0	>50	JAK3@2	0	>50
SLK	1	**0.7**	**SLK**	0.3	**1.2**
DCAMKL3	11	>50	ICK	1.3	>50
GSK3A	12	5.3	DCAMKL3	2.3	>50
TLK2	13	>50	SNARK	5.8	ND
TLK1	13	>50	**STK10**	7.3	**1.5**
MAP2K5	15	ND	GSK3A	9.4	14
YSK1	15	>50	YSK1	9.8	>50
STK3	16	17	TLK2	10	>10
STK10	16	**1.4**	CDK7	11	>50
CLK2	23	1.8	CLK2	17	8.4
CLK4	45	4.4	CLK4	26	7.7

Table 6. Kinome selectivity analysis of compounds **31** and **41** (DiscoverX KINOMEscan) and verification in cells by NanoBRET assay. The top 10 kinases identified as binding to the compounds in KINOMEscan are listed, in addition to CLK2 and CLK4; full datasets are available in the Supplementary Material. ND = not determined. Example NanoBRET binding curves can be seen in Supplementary Figure 2. Note that a different tracer compound was used for STK10 and SLK NanoBRET measurements compared to that used for compounds **2** and **4** above.

Aiming to improve potency through interaction in a predicted pocket in the binding site (based on docking models, data not shown) as well as determine the size of aniline substituents that would be tolerated a further series of modifications on the aniline ring was performed (Table 7). Overall, while all substituents were tolerated, no increase in potency was obtained although **51** and **53** were comparable. However, it is interesting to highlight from this series the behavior of **56** (K_i = 37 nM) and **57** (K_i = 120 nM) in which the ketone-linker derivative is ~3.2-fold more potent than the NH-linker, perhaps due to conformational rigidity. A 3-thienyl substituent at the *para* position (**59**: K_i = 43 nM) was ~2.5-fold more potent compared with the same substituent in the *meta* position (**58**: K_i = 110 nM). Meanwhile, the most significant difference was found between the 6-quinolyl (**63**: K_i = 17 nM) and 8-quinolyl (**64**: K_i = 370 nM) derivatives; the former was ~21-fold more potent than the latter.

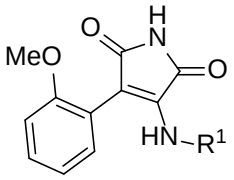

Compound	R_1	K_i (nM)		STK10/SLK
		SLK	STK10	
51	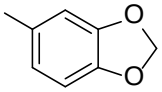	15	84	5.8
52	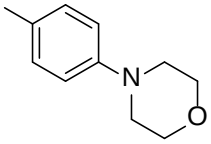	47	460	9.8
53	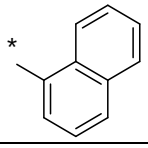	6.0	47	7.8
54	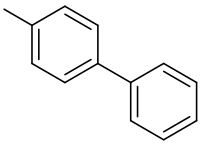	25	320	13
55	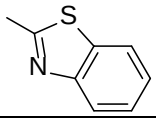	1100	7300	6.6
56	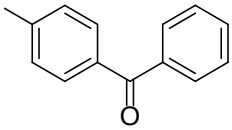	37	600	16
57	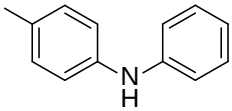	120	1200	10

58	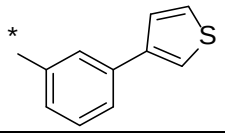	110	640	5.8
59	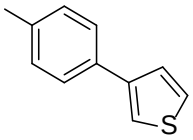	43	400	9.3
60	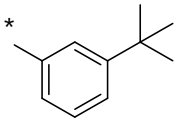	1400	5500	3.9
61	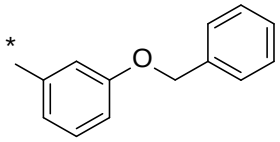	510	3200	6.3
62	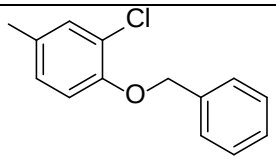	170	790	4.6
63	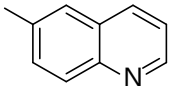	17	110	6.5
64	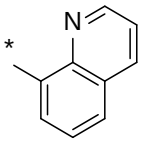	370	1500	4.1
65	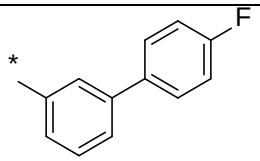	1500	6900	4.6

Table 7. K_i values were determined in a binding displacement assay.

Co-crystal structures reveal the binding mode in the ATP site

At this stage we were successful at co-crystallizing SLK and STK10 with compounds **55** and **56** respectively, enabling a determination of the co-crystal structures of SLK:**55** and STK10:**56** (Supplemental Table 1). The structures revealed a similar binding mode of the compounds in the ATP binding sites of SLK and STK10 (Figure 1), with the maleimide group forming two hydrogen bonds with the kinase hinge (at E109 and C111 in SLK, and E111 and C113 in STK10). The aniline and aryl substituents are rotated to a similar angle relative to the maleimide group in each so that the aniline group is almost stacked over the methoxy of the aryl ring. The maleimide forms a hydrogen-bonding interaction with a water molecule in the back of the ATP binding pocket that bridges between the ligand and the amide backbone of the "DFG" motif aspartate residue, conserved between the structures (Figure 1A, 1B). There is a further interaction with a conserved water

molecule at the front of the ATP pocket and the ligand. Numerous hydrophobic interactions between the ligand and hydrophobic side chains of residues in the ATP binding pocket are evident. In the STK10:**56** structure, the methoxy-phenyl moiety interacts with V50, the maleimide group is sandwiched between A63 and L164, and the benzyoylphenyl-amino moiety makes extended contacts with the flexible glycine-rich loop at L42-F47, forcing the loop upwards relative to the SLK:**55** structure. In the SLK structure, similar hydrophobic contacts are made between residues L40, V48, A61, L162, A172 and the ligand, but with a more closed conformation of the glycine-rich loop.

There are several other kinase-maleimide structures available in the PDB, and comparison with these structures may explain some of the identified cross-reactivity of this compound series. For example, structures of GSK3β in complex with maleimide inhibitors (PDB IDs 1q4l, 1r03, 2ow3) retain many of the binding features described above, such as the polar interaction of the maleimide group with both the hinge and with a bridging water molecule at the back of the ATP pocket. One of the crystallized compounds is a large macrocyclic maleimide inhibitor (PDB ID 2ow3), demonstrating that GSK3β is capable of binding even very bulky compounds. It is, therefore, not surprising that GSK3β and the closely related GSK3α were observed as off-targets of inhibitors **1**, **31** and **41** (Tables 1, 5 and 6).

CLK2 was found to be an off-target of compound **1** by KINOMEscan (Table 1) and comparison of CLK2 structures with the SLK:**55** structure confirms that many residues interacting with maleimide and methoxy-phenyl groups are conserved between the binding sites of these kinases, including V177, A191, L297 in CLK2, equivalent to V48, A61, L162 in SLK.

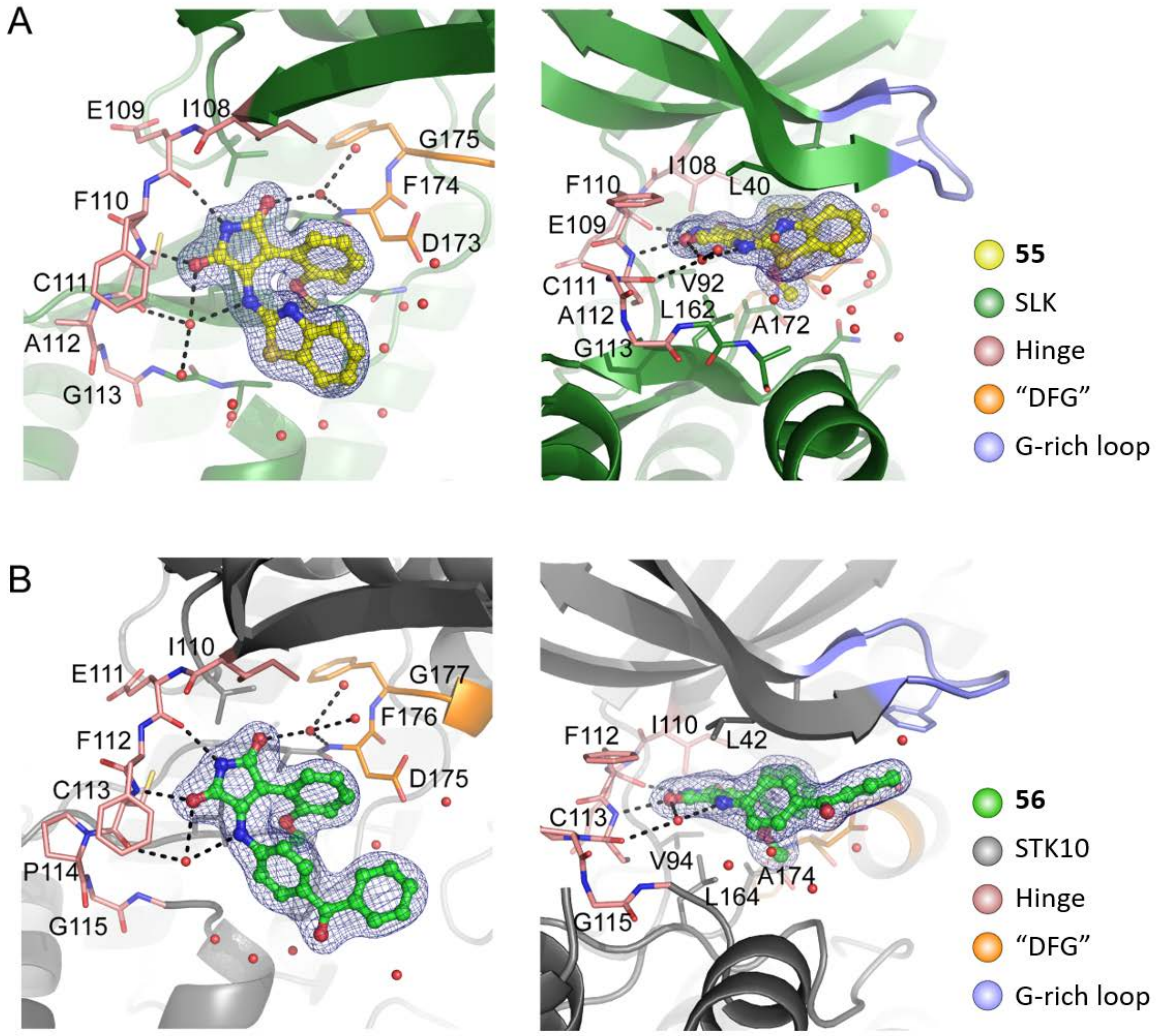

Figure 1. Co-crystal structures of SLK and STK10 with maleimide inhibitors bound at the ATP-binding pocket. **A.** Compound **55** bound to SLK (PDB ID 6HVD) and **B.** Compound **56** bound to STK10 (PDB ID 6HXF). A $2F_o$-F_c electron density map is shown as a blue mesh contoured at 1 σ around the ligand. Polar contacts are illustrated by black dotted lines. Red spheres indicate positions of water molecules. Strands β1-β3 have been removed from the left panels for clarity.

Structure-guided inhibitor development

Based on the co-crystal structures a virtual library of maleimides was docked and evaluated with the aim of acquiring new interactions with the kinase P-loop region by adding substituents to the *meta* and *para* positions of the aryl ring (Table 8), while maintaining the most potent aniline ring substituent (*meta*-CN). Smaller modifications such as phenyl (**66**,**67**), thiophene (**74**,**75**), pyridine (**76**-**78)**, isobutyramide (**79**,**80**) and

bromide (**81**,**82**) were much better tolerated than bulkier groups (**68**-**73**). The most potent compounds from this set were the bromide derivatives **81** (K_i = 3.9 nM) and **82** (K_i = 9.7 nM), with **81** equipotent with the previous most potent compounds **31** and **41**.

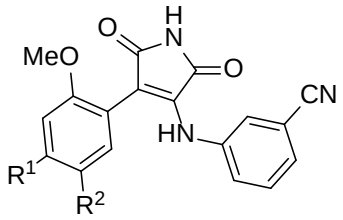

Cmpd	R_1	R_2	K_i (nM)		STK10 /SLK
			SLK	STK10	
66	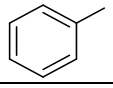	H	330	3000	9.1
67	H	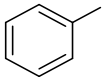	40	320	8.0
68	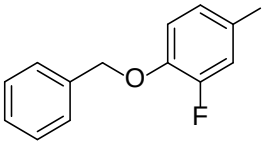	H	3000	NB	-
69	H	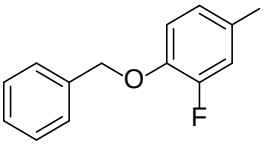	380	2000	5.3
70	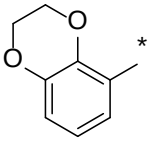	H	720	4600	6.4
71	H	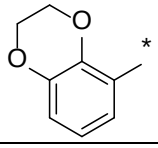	840	4600	5.5
72	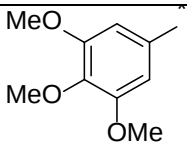	H	2100	NB	-
73	H	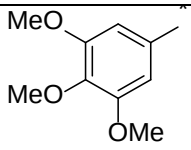	1100	3700	3.4
74		H	180	540	3.0
75	H		520	1100	2.1

76	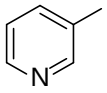	H	240	440	1.8
77	H	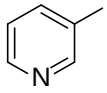	680	1900	2.8
78	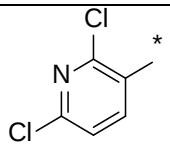	H	30	320	10.7
79	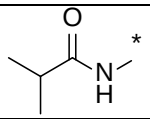	H	17	88	5.2
80	H	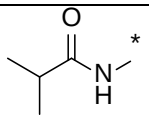	15000	NB	-
81	Br	H	3.9	35	9.0
82	H	Br	9.7	61	6.3

Table 8. K_i values were determined in a binding displacement assay. NB = no binding (>100 µM).

Selectivity, *in vitro* and cellular potency

The kinome selectivity of the newly identified potent inhibitors **53**, **81** and **82** was assessed (Table 9). These data suggested that **53** was potentially more selective than **31** or **41** although SLK did not feature in the top hits despite a potent IC_{50} value in our *in vitro* assay. **81** was similarly selective (S_{35} = 0.045) as was **82** when screened at the lower concentration of 100 nM. We therefore sought to confirm the *in vitro* and cellular potency and cellular selectivity for these inhibitors.

To verify the ability of **31**, **41**, **53**, **81** and **82** to inhibit the enzymatic activity of a full-length kinase we established an OMNIA assay to measure the activity of full length STK10 (Table 9), which again demonstrated low nM range inhibition by compounds **31** and **41** and slightly weaker inhibition by **81** and **82** while **53** was much weaker, in accordance with the selectivity data. The ranking of these inhibitors was matched in cells where **31** and **41** were the most potent, having IC_{50} values against STK10 of 1.4 and 1.5 µM respectively, and IC_{50} values against SLK of 0.7 and 1.2 µM respectively.

Taking all data together compound **31** therefore represents the best combination of cellular potency and selectivity yet achieved for an SLK and STK10 inhibitor.

Compound	**31**	**41**	**53**	**81**	**82**
STK10 *in vitro* IC_{50} (nM)[a]	12 ± 2	23 ± 8	1420 ± 270	60 ± 61	99 ± 84
STK10 cellular IC_{50} (μM)[b]	1.4[e]	1.5[e]	>20	4.4	4.5
SLK cellular IC_{50} (μM)[b]	0.7[e]	1.2[e]	>20	17	19
Selectivity Score (S_{35})	0.040[c]	0.062[c]	0.047[d]	0.045[c]	0.005[d]

Table 9. Characterization of the most potent identified SLK and STK10 inhibitors. [a] IC_{50} measurements for the inhibition of STK10 at [ATP] = 60 μM. Values are the mean and standard deviation from two independent determinations. [b] NanoBRET measurements in HEK293T cells. [c] Selectivity score calculated as the number of kinases below N% of control divided by the total number of kinases, from compounds screened at 1.0 μM. [d] At 0.1 μM. [e] As in Table 6.

Effect on moesin phosphorylation and cell migration

Both SLK and STK10 were previously shown to phosphorylate the ezrin/radixin/moesin (ERM) proteins and it was previously shown that in lymphocytes from STK10 knockout mice there was a 50% reduction in ERM phosphorylation[1]. The ERM phosphorylation by STK10 was shown to be an important step in the activation of the ERM proteins[15] and we previously showed with a different class of inhibitor that chemical inhibition of STK10 and SLK could diminish the pMoesin/moesin ratio[19]. Furthermore, kinase inhibitors affect protein conformation and can have effects beyond inhibition of catalytic activity, and given the importance of interactions of STK10 and SLK for various aspects of cell polarity/shape/migration as well as the additional known substrates of SLK/STK10 such as PLK1, the cellular effects of chemical inhibition of SLK/STK10 cannot be predicted with certainty. Nevertheless, the observations that SLK is essential for breast cancer cell motility[21], increased SLK expression is associated with increased prostate cancer cell migration[22], and decreased SLK expression is associated with decreased glomerular epithelial cell migration[23] and decreased fibroblast migration[24] suggested that chemical inhibition would be likely to decrease cell migration. The previous observation that erlotinib, which potently inhibits both SLK and STK10 among many other targets, also decreased glomerular epithelial cell migration[23] further suggested that specific inhibition of SLK/STK10 might decrease cell migration.

Therefore, as an initial investigation into the effect of chemical inhibition of SLK/STK10, and to validate the use of **31** for investigating the roles of SLK and STK10, we tested the ability of **31** to affect cellular migration and to inhibit moesin phosphorylation by SLK and STK10 (Figure 2). The data show that **31** inhibited cellular migration of CAL51 cells in a dose-dependent manner with a maximal effect at ~10 μM and a half-maximal effect (EC_{50}) of ~1 μM, although only the 10 μM dose reached $p < 0.05$ (Figure 2A). The recovered cells showed a reduction in the ratio of pMoesin/moesin of around 30% in the presence of **31** compared to untreated control (Figure 2B).

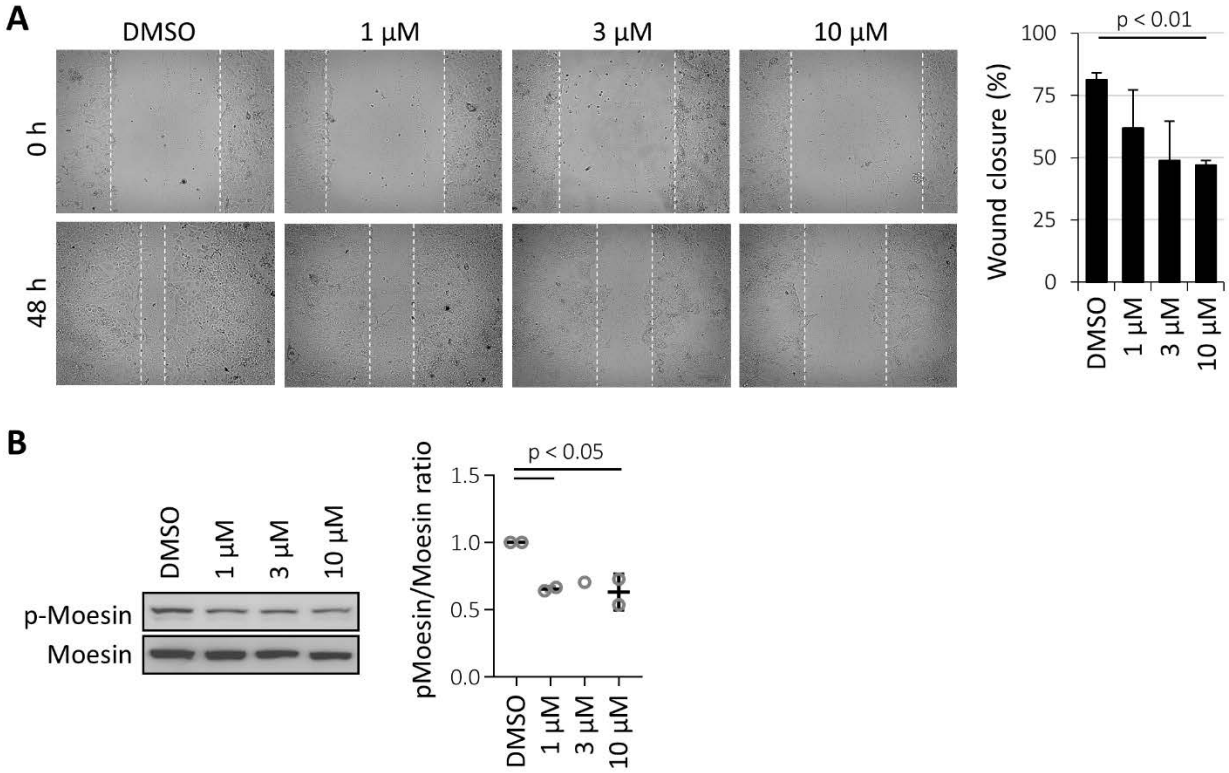

Figure 2. Inhibition of SLK/STK10 impairs cell migration and cellular pMoesin:Moesin levels. **A** CAL51 cells were scratched and imaged at 0 h and 48 h in the absence and presence of **31** (image panels). The distance created by scratching was determined at multiple (≥5) regions along the cleared area at 0 h and 48 h using ImageJ. The data were normalised to the distance at 0 h for each condition and plotted using Excel (bar chart). A standard *t*-test was performed to determine the significance between DMSO and 10 µM. **B** Representative Western blot (left) of pMoesin and moesin and analysis of 2 independent experiments (right) of the scratched cells after 48 h from A. One of the samples for the 3 µM data points was lost during generation. One-way ANOVA (multiple comparisons) was performed to determine significance.

Discussion and Conclusions

The good selectivity of several inhibitors from this series is somewhat surprising considering that maleimides are an often poorly selective kinase inhibitor scaffold. The crystal structures of STK10 and SLK with this series demonstrate that the essential *ortho* substituent on the aryl ring (methoxy or chloro) occupies a small pocket on the bottom of the ATP-binding pocket, between conserved leucine and glutamine residue (SLK Leu162 and Asn160, Figure 1). The SAR analysis demonstrated the importance of the *ortho* methoxy or chloro, and it is therefore likely that binding to this small pocket is important for the potency of this series for STK10 and SLK. Furthermore, the hydrogen bonding of the maleimides to two structural water molecules, one on each side of the inhibitor (Figure 1), is conserved between STK10 and SLK. Binding to a structural water molecule on each side of the inhibitor implies that the distance between these two water molecules is important for the binding strength of the inhibitor. Presumably this geometry of the ATP binding site and placement of water molecules is only possible in STK10, SLK and perhaps the few off-target kinases identified in the cross-screening experiments.

It is reassuring that the inhibitors showed similar potency *in vitro* in enzymatic assays at [ATP] = K_M(ATP) as in the binding-displacement assay. The concordance of results between these two assay formats increases confidence that, since the inhibitors were shown to directly bind STK10 and SLK in cells, they will inhibit the enzymatic activity of STK10 and SLK in cells, and indeed it is further reassuring that **31** was able to inhibit moesin phosphorylation in cells, showing a convincing effect at 1 μM, as well as demonstrate a convincing effect on cellular migration. It is important to note that the true cellular IC_{50} of the compounds will be lower than that measured in the NanoBRET assay, in which the inhibitor competes with a fluorescent tracer molecule for binding to the kinase, in addition to the competition with ATP.

While **31** is a potent inhibitor of SLK and STK10 with good overall kinome selectivity, several off-target kinases are affected in cells with an IC_{50} <10x that of SLK/STK10, which would complicate using **31** for associating SLK or STK10 with cellular phenotypes. In particular, inhibition of CLKs may have significant effects on resulting cellular phenotypes due to the role of these kinases in regulating alternate splicing. Off-target inhibition of the highly networked kinases GSK3α or GSK3β by **31** may also be an issue[25]. Thus, further optimization will be needed to convert these molecules into exclusively selective tools for studying the cellular biology of SLK and STK10.

Experimental Section

Kinome selectivity profiling

Inhibitors were profiled against the kinase panel (KINOMEscan) of DiscoverX Corporation (California, USA) at a concentration of 1.0 µM, except for compound **82** which was profiled at 0.1 µM.

Protein Expression and Purification for Crystallization

Kinase domain constructs of $STK10_{(R18\text{-}E317)}$ and $SLK_{(R26\text{-}E320)}$ were cloned into an expression vector (pNIC28-Bsa4) that adds an N-terminal hexahistidine tag and a TEV protease recognition site for removal of the tag. To produce the unphosphorylated kinases, the proteins were co-expressed together with bacteriophage lambda phosphatase. Cells were grown to an OD_{600} of 0.4-0.5 at 37 °C in LB medium (Miller), then the temperature was lowered to 20 °C. Protein expression was induced by the addition of 0.5 mM isopropyl 1-thio-D-galactopyranoside at an OD_{600} of 0.6 and allowed to proceed overnight. Cells were harvested by centrifugation and resuspended in 15 mL of buffer A (50 mM HEPES pH 7.4, 500 mM NaCl, 5 % glycerol, 0.5 mM TCEP) supplemented with 20 mM imidazole per 1 L of culture and stored frozen at -20 °C until required. For purification of the proteins, the thawed cells were lysed by sonication on ice and polyethylenimine was added to a final concentration of 0.15% prior to clarification by centrifugation. The supernatant was loaded onto nickel-sepharose beads pre-equilibrated in buffer A in a gravity-flow column. The column was washed with buffer A supplemented with a sequentially increasing concentration of imidazole and fractions collected. The fractions containing the target protein were pooled and dialyzed overnight with TEV protease at 4 °C for cleavage of the affinity tag, then further purified using nickel affinity chromatography and size-exclusion chromatography. The proteins were concentrated to >10 mg/mL using an Amicon Ultra 30 kDa MWCO centrifugal filter device prior to crystallization.

Crystallization and Structure Determination

Purified STK10 or SLK was mixed with 1 mM of inhibitor compound and crystallized by vapor-diffusion in 150 nL volume sitting drops equilibrated at 4 °C against 20 µL of reservoir solution. Diffraction-quality crystals were found using protein:precipitant ratios of 1:1 and 1:2. Crystals were cryo-protected by addition of a reservoir solution supplemented with 25% ethylene glycol, then harvested and flash frozen in liquid nitrogen. Data was collected at Diamond Light Source beamline i04-1 using a DECTRIS Pilatus 6M-F detector. Data reduction and scaling was performed using XDS[26] and AIMLESS[27]. Structures were solved by molecular replacement using the search models described in Supplementary Table 2 using Phaser[28] and refinement was

carried out using REFMAC[29], Phenix[30] and Coot[31]. Data processing and refinement statistics for the final models are given in Supplementary Table 2.

Binding-displacement assays

IC_{50} values for inhibitor binding to STK10 or SLK kinase domain proteins were determined using a binding-displacement assay in which the ability of the inhibitors to displace a fluorescent tracer molecule was measured, as previously described[32].

NanoBRET measurements

NanoBRET measurements of compounds **2** and **4** with STK10 or SLK were made in HEK293 cells. 1 mL of 9 µg/mL transfection carrier DNA and 1 µg/mL Nanoluc fusion of STK10 or SLK (Promega) was mixed with 30 µL FuGENE HD (Promega), incubated for 20 mins and added to 20 mL of HEK293 cells at 2 x 10^5 cells/mL in Opti-MEM media. The cells were incubated in a T75 flask at 37 °C, 5% CO_2 for 20 hours. The medium was removed by aspiration, the cells were washed with 5 mL PBS and then detached with trypsin. 3 mL medium was added and the cells were centrifuged at 200 x g for 5 minutes. The cells were resuspended in media containing 30 µM extracellular NanoLuc inhibitor (Promega) and the cell density was adjusted to 2 x 10^5 cells/mL. 85 µL was added to each well of a white 96-well plate (Greiner). 5 µL of 20x Tracer 5 (Promega) was added to each well and mixed carefully. A serial dilution at 10x final concentration of each inhibitor was prepared in DMSO and 10 µL of each serial dilution was added to a well. The plate was incubated at 37 °C, 5% CO_2 for 2 hours, transferred to room temperature and 50 µL of 3x Nano-Glo substrate was added to each well. BRET measurements were made on a PHERAstar FS plate reader (BMG LabTech) at 610 nm and 480nm.

NanoBRET measurements for other compounds and kinases were made similarly except that HEK293T cells and 384-well plates (Greiner) were used for the measurements and BRET measurements were made using a PHERAstar FSX plate reader (BMG LabTech) equipped with 450 nm BP filter (donor) and 610 nm LP filter (acceptor). NanoBRET materials and tracer concentrations used can be found in Supplementary Table 3. Competitive displacement data was then analysed using GraphPad Prism 8 software using a 3-parameter curve fit with the following equation: Y=100/(1+10^(X-Log(IC50))) where data was normalized to background and tracer only control signal.

Purification of full length STK10 protein

DNA encoding biotinylated full-length STK10 (1-968) was cloned into a baculovirus transfer vector (pFB-Bio5) that adds an N-terminal hexahistidine tag and a TEV protease recognition site for removal of the tag, and encodes BirA protein with a signal peptide for co-expression. To produce the biotinylated full-length

kinases, the expression construct was transformed into *E. coli* DH10Bac competent cells, which were used to prepare recombinant bacmid DNA. The bacmid DNA was then transfected into *Spodoptera frugiperda* insect cells (*Sf9)* from which recombinant baculovirus was recovered. After three cycles of amplification of the virus, *Sf9* cells at 2 million cells per mL were infected with virus in media containing 15 mL/L of filter-sterilised 10 mM biotin solution. Expression was carried out for 72 hours at 27 °C. The cells were harvested by centrifugation at 900 x g, re-suspended in buffer A and frozen at -20 °C until further use, then purified by nickel affinity chromatography and SEC similar to the kinase domain constructs, with removal of the hexahistidine tag by addition of TEV, as before. Protein identity was confirmed using MS-MS, denaturing intact LC-MS and SDS-PAGE. Protein was found to be heavily auto-phosphorylated by LC-MS.

Enzymatic IC_{50} measurements

Enzymatic assays involving measurement of the transfer of radiolabeled phosphate from ATP were performed by Reaction Biology Corporation. In this assay the ATP concentration used was 10 µM, and the *K*m(ATP) values for STK10 and SLK were 700 µM and 13 µM respectively.

OMNIA enzymatic assays were performed per the manufacturer's indications (AssayQuant). Recombinant *Sf9*-expressed STK10 kinase domain (KD) or full-length (FL) in 10 mM $MgCl_2$, 50 mM HEPES pH 7.5, 0.01 % Tween 20, 0.2 mg/mL BSA, 1 mM DTT, 1% Glycerol were both used at a concentration of 5 nM. ATP titration in a range of 2.5 mM to 250 nM was performed at 1 µM STK10-SOX peptide (AssayQuant) present. Assays were performed in 20 µL reactions in white 384-well plates (Greiner #781075) at 1 mM ATP or 60 µM ATP (K_M(ATP) for both protein constructs, previously determined). For the K_M(ATP) or inhibitor IC_{50} determination the fluorescence of the STK10-SOX peptide after 360 nm excitation was monitored for 1 h at 487 nm emission in a PHERAstar FSX platereader (BMG Labtech) and the linear portion of the curves (10% of maximum signal) was then fitted using GraphPad Prism 8 "straight line"-fit. The resulting slopes were plotted against the logarithmized ATP or inhibitor concentration to provide a Michaelis-Menten Diagram or IC_{50} diagram, respectively, that was fitted using GraphPad Prism 8 Michaelis-Menten Fit or normalized 3-parameter-fit model.

Cell migration and western blot analysis

CAL51 cells grown to confluence under standard conditions (DMEM, Glutamine, 10% serum at 37 °C and 5% CO_2) and then serum starved overnight were scratched to assess cell migration. Cells were washed twice in serum free media and imaged immediately and at 48 hours afterwards. Cells were then washed twice on ice with PBS buffer (4 °C) and protein lysate isolated using standard RIPA buffer with phosphatase and protease inhibitors (Roche). Cell debris was removed and samples run out using SDS-PAGE, transferred and

probed as stated. Antibodies used were anti-Moesin (Abcam, ab52490) and anti-phospho Moesin (Abcam, ab177943). Quantification of blots was carried out using ImageJ.

Chemistry

General: All assayed compounds were characterized by ^{1}H NMR, ^{13}C NMR and HRMS. In all cases, compound purity was found to be ≥95%. (for further details, see S*upporting Information*).

General procedure for the 4-hydroxymaleimide intermediate generation: At a temperature of 0 °C, *t*-BuOK (1 M in THF, 2 equiv.) was added dropwise to a THF (0.14 M) solution of diethyl oxalate (1.1 equiv.) and acetamide (1 equiv.). The reaction mixture was stirred at room temperature for 4 h, and then it was poured into 1 M aqueous hydrochloric acid solution. The mixture was extracted with ethyl acetate. The organic phase was successively washed with brine, dried over Na_2SO_4, and concentrated under reduced pressure to afford the maleimide scaffold, which was used for the next step without any previous purification.

General procedure for the last step of synthesis of all final compounds (9-82): 4-hydroxymaleimide (1 equiv.) and aniline or benzylamine (1.05 equiv.) were combined in acetic acid (0.26 M) and stirred for 12 h at 100 °C. After all starting material had been consumed, the mixture was extracted with water/ethyl acetate. The organic phase was combined, dried over Na_2SO_4 and purified by silica flash chromatography using a gradient of 10%-80% ethyl acetate in hexane.

General procedure for Fischer-Speier esterification and generation of subsequent acetamide intermediates (**I**, **II**, **XI**, **XII**) (*Part A* and *B*):

Part A: The respective carboxylic acid derivative (1.0 equiv.) was mixed with methanol (0.4 M) and H_2SO_4 (2 drops/mmol of carboxylic acid derivative) and stirred under reflux for 10 h. After all starting material had been consumed, the mixture was concentrated under reduced pressure. An extraction using water/ethyl acetate was performed, and the organic phase was combined, dried over Na_2SO_4 and concentrated again under reduced pressure to obtain the desired product, which was directly submitted to the *Part B*. A portion of the material was used for the Buchwald-Hartwig coupling reaction before acetamide generation.

Part B: The respective ester derivative (1.0 equiv.) was mixed with methanol (0.23 M) and ammonium hydroxide solution 30% (0.13 M) and stirred at 80 °C for 10 h. After all starting material had been consumed, the mixture was concentrated under reduced pressure. Extraction using brine/ethyl acetate was performed, and the organic phase was combined, dried over Na_2SO_4 and concentrated again under reduced pressure to obtain the desired acetamide.

General procedure for intermediates (III-XIII) resulting from Suzuki-Miyaura coupling:

A vial equipped with a magnetic stirrer bar was charged with Cs_2CO_3 (2.5 equiv.), $Pd(dppf)Cl_2$ (10 mol%), the respective boronic acid (1.1 equiv.), the respective acetamide bromide (1 equiv.) and a mixture of 1,4-dioxane/water 5:1 (0.25 M) as solvent system (previously degassed in an ultrasonic bath). The reaction mixture was stirred at 85 °C for 7 h. After cooling to room temperature, the material was filtered through a pad of diatomaceous earth with ethyl acetate and methanol as washing solvent. The product was purified by silica flash chromatography using a gradient of 40% ethyl acetate in hexane to 5% methanol in ethyl acetate.

General procedure for intermediates (XIV-XV) resulting from Buchwald-Hartwig coupling:

A vial equipped with a magnetic stirrer bar was charged with Cs_2CO_3 (2.5 equiv.), $Pd_2(dba)_3$ (10 mol%), XantPhos (20 mol%), isobutyramide (1.1 equiv.), the respective ester bromide (1.0 equiv.) and dry 1,4-dioxane (0.2 M) as solvent system (previously degassed in an ultrasonic bath). The reaction mixture was stirred at 85 °C for 8 h. After cooling to room temperature, the material was filtered through a pad of diatomaceous earth with ethyl acetate as washing solvent. The product was purified by silica flash chromatography using a gradient of 20% to 60% ethyl acetate in hexane.

3-((2-(methylthio)phenyl)amino)-4-(2-(trifluoromethyl)phenyl)-1H-pyrrole-2,5-dione (9).

Compound **9** was isolated as a yellow solid in 22% yield. ^{1}H NMR (400 MHz, DMSO-d_6) δ 10.72 (s, 1H), 8.86 (s, 1H), 7.47 – 7.43 (m, 1H), 7.31 – 7.24 (m, 2H), 7.08 – 7.04 (m, 1H), 7.00 – 6.91 (m, 2H), 6.70 – 6.62 (m, 2H), 2.37 (s, 3H). ^{13}C NMR (101 MHz, DMSO-d_6) δ 172.12, 168.24, 141.45, 135.81, 134.12, 132.55, 130.91, 128.66, 128.36 (d, J = 1.9 Hz), 128.01, 127.04, 126.59, 125.43 (q, J = 4.9 Hz), 125.31, 125.14, 123.94, 122.58, 99.15, 14.34. HRMS (ES): calcd for $C_{18}H_{13}F_3N_2O_2S$ $[M+H]^+$: 379.0728. Found: 379.0717.

3-(2-chlorophenyl)-4-((2-(methylthio)phenyl)amino)-1H-pyrrole-2,5-dione (10).

Compound **10** was isolated as a yellow solid in 58% yield. ^{1}H NMR (400 MHz, DMSO-d_6) δ 10.73 (s, 1H), 8.86 (s, 1H), 7.12 – 7.05 (m, 2H), 7.02 – 6.98 (m, 2H), 6.95 (ddt, J = 5.6, 3.7, 2.8 Hz, 2H), 6.71 – 6.64 (m, 2H), 2.35 (s, 3H). ^{13}C NMR (101 MHz, DMSO-d_6) δ 171.77, 168.32, 140.93, 134.87, 134.21, 133.84, 131.86, 129.15, 128.86, 128.08, 126.61, 125.70, 125.42, 125.36, 123.92, 99.58, 14.63. HRMS (ES): calcd for $C_{17}H_{13}ClN_2O_2S$ $[M+H]^+$: 345.0465. Found: 345.0455.

3-(2-methoxyphenyl)-4-((2-(methylthio)phenyl)amino)-1H-pyrrole-2,5-dione (11).

Compound **11** was isolated as a yellow solid in 60% yield. ^{1}H NMR (400 MHz, DMSO-d_6) δ 10.70 (s, 1H), 8.21 (s, 1H), 7.18 – 7.07 (m, 3H), 6.92 (t, J = 6.2 Hz, 1H), 6.82 (t, J = 7.5 Hz, 1H), 6.59 (t, J = 7.7 Hz, 1H), 6.50 (d, J = 8.0 Hz, 1H), 6.38 (d, J = 7.9 Hz, 1H), 3.24 (s, 3H), 2.42 (s, 3H). ^{13}C NMR (101 MHz, DMSO-d_6) δ 172.56, 168.91, 156.55, 138.56, 134.97, 131.97, 130.53, 128.91, 125.98, 125.15, 123.87, 122.51, 119.16, 118.74, 109.67, 99.08, 54.35, 15.06. HRMS (ES): calcd for $C_{18}H_{16}N_2O_3S$ $[M+H]^+$: 341.0960. Found: 341.0947.

3-((3-(methylthio)phenyl)amino)-4-(2-(trifluoromethyl)phenyl)-1H-pyrrole-2,5-dione (12).

Compound **12** was isolated as a yellow solid in 38% yield. ^{1}H NMR (400 MHz, DMSO-d_6) δ 10.77 (s, 1H), 9.35 (s, 1H), 7.50 (d, *J* = 7.8 Hz, 1H), 7.44 (t, *J* = 7.5 Hz, 1H), 7.36 (t, *J* = 7.6 Hz, 1H), 7.19 (d, *J* = 7.6 Hz, 1H), 6.81 (t, *J* = 7.9 Hz, 1H), 6.69 (ddd, *J* = 7.9, 1.8, 1.0 Hz, 1H), 6.62 (t, *J* = 1.9 Hz, 1H), 6.54 (ddd, *J* = 8.0, 2.0, 0.8 Hz, 1H), 2.23 (s, 3H). ^{13}C NMR (101 MHz, dmso) δ 172.31, 168.56, 140.21, 137.93, 132.77, 131.60, 129.53 (d, *J* = 2.1 Hz), 128.56, 128.28, 128.13, 127.99, 125.79 (q, *J* = 4.7 Hz), 125.26, 122.53, 121.72, 120.28, 119.28, 99.56, 14.57. HRMS (ES): calcd for $C_{18}H_{13}F_3N_2O_2S$ $[M+H]^+$: 379.0728. Found: 379.0717.

3-(2-chlorophenyl)-4-((3-(methylthio)phenyl)amino)-1H-pyrrole-2,5-dione (13).

Compound **13** was isolated as a yellow solid in 62% yield. ^{1}H NMR (400 MHz, DMSO-d_6) δ 10.82 (s, 1H), 9.57 (s, 1H), 7.22 – 7.11 (m, 4H), 6.89 – 6.83 (m, 1H), 6.76 – 6.70 (m, 1H), 6.58 (tt, *J* = 3.1, 1.5 Hz, 2H), 2.23 (s, 3H). ^{13}C NMR (101 MHz, DMSO-d_6) δ 171.90, 168.58, 139.59, 138.05, 137.79, 133.93, 131.92, 129.99, 129.27, 128.59, 127.90, 126.31, 121.38, 119.04, 118.46, 100.00, 14.41. HRMS (ES): calcd for $C_{17}H_{13}ClN_2O_2S$ $[M+H]^+$: 345.0465. Found: 345.0455.

3-(2-methoxyphenyl)-4-((3-(methylthio)phenyl)amino)-1H-pyrrole-2,5-dione (14).

Compound **14** was isolated as a yellow solid in 57% yield. ^{1}H NMR (400 MHz, DMSO-d_6) δ 10.70 (s, 1H), 9.35 (s, 1H), 7.26 (dd, *J* = 7.6, 1.7 Hz, 1H), 7.18 (ddd, *J* = 8.4, 7.4, 1.8 Hz, 1H), 6.94 – 6.85 (m, 2H), 6.71 (ddd, *J* = 7.8, 1.7, 0.9 Hz, 1H), 6.62 – 6.54 (m, 2H), 6.43 (t, *J* = 1.9 Hz, 1H), 3.10 (s, 3H), 2.09 (s, 3H). ^{13}C NMR (101 MHz, DMSO-d_6) δ 172.75, 169.17, 156.52, 138.78, 137.83, 137.47, 130.39, 129.13, 127.62, 120.50, 119.50, 119.34, 117.24, 109.90, 98.99, 54.35, 14.16. HRMS (ES): calcd for $C_{18}H_{16}N_2O_3S$ $[M+H]^+$: 341.0960. Found: 341.0950.

3-((4-(methylthio)phenyl)amino)-4-(2-(trifluoromethyl)phenyl)-1H-pyrrole-2,5-dione (15).

Compound **15** was isolated as a yellow solid in 37% yield. ^{1}H NMR (400 MHz, DMSO-d_6) δ 10.77 (s, 1H), 9.40 (s, 1H), 7.54 – 7.45 (m, 2H), 7.40 (t, *J* = 7.5 Hz, 1H), 7.21 (d, *J* = 7.5 Hz, 1H), 6.77 (d, *J* = 8.7 Hz, 2H), 6.70 (d, *J* = 8.7 Hz, 2H), 2.30 (s, 3H). ^{13}C NMR (101 MHz, DMSO-d_6) δ 172.28, 168.53, 140.63, 134.69, 133.41, 133.03, 131.58, 129.68 (d, *J* = 2.1 Hz), 128.75, 128.46, 128.19, 125.74, 125.66, 125.22, 123.39, 122.49, 98.95, 15.35. HRMS (ES): calcd for $C_{18}H_{13}F_3N_2O_2S$ $[M+H]^+$: 379.0728. Found: 379.0716.

3-(2-chlorophenyl)-4-((4-(methylthio)phenyl)amino)-1H-pyrrole-2,5-dione (16).

Compound **16** was isolated as an orange solid in 62% yield. ^{1}H NMR (400 MHz, DMSO-d_6) δ 10.74 (s, 1H), 9.56 (s, 1H), 7.19 – 7.11 (m, 3H), 7.10 – 7.06 (m, 1H), 6.75 (d, *J* = 8.7 Hz, 2H), 6.64 (d, *J* = 8.7 Hz, 2H), 2.27 (s, 3H). ^{13}C NMR (101 MHz, DMSO-d_6) δ 171.88, 168.55, 139.99, 134.71, 133.98, 132.91, 132.01, 130.12, 129.12,

128.43, 126.28, 125.59, 122.49, 99.39, 15.49. HRMS (ES): calcd for $C_{17}H_{13}ClN_2O_2S$ $[M+H]^+$: 345.0465. Found: 345.0454.

3-(2-methoxyphenyl)-4-((4-(methylthio)phenyl)amino)-1H-pyrrole-2,5-dione (17).

Compound **17** was isolated as an orange solid in 58% yield. ^{1}H NMR (400 MHz, DMSO-d_6) δ 10.65 (s, 1H), 9.37 (s, 1H), 7.19 (t, *J* = 7.7 Hz, 2H), 6.90 (t, *J* = 7.4 Hz, 1H), 6.79 (d, *J* = 8.5 Hz, 2H), 6.61 (d, *J* = 8.5 Hz, 2H), 6.53 (d, *J* = 8.1 Hz, 1H), 3.12 (s, 3H), 2.31 (s, 3H). ^{13}C NMR (101 MHz, DMSO-d_6) δ 172.67, 169.14, 156.55, 138.29, 135.58, 131.57, 130.34, 128.95, 125.85, 121.14, 119.60, 119.38, 109.82, 98.56, 54.43, 15.96. HRMS (ES): calcd for $C_{18}H_{16}N_2O_3S$ $[M+H]^+$: 341.0960. Found: 341.0949.

3-(2-chlorophenyl)-4-((3-(methylsulfonyl)phenyl)amino)-1H-pyrrole-2,5-dione (18).

Compound **18** was isolated as a yellow solid in 40% yield. ^{1}H NMR (400 MHz, DMSO-d_6) δ 10.91 (s, 1H), 9.88 (s, 1H), 7.41 – 7.37 (m, 1H), 7.26 (t, *J* = 1.9 Hz, 1H), 7.19 (dddd, *J* = 8.7, 7.3, 4.3, 3.1 Hz, 5H), 7.09 (ddd, *J* = 8.1, 2.2, 1.0 Hz, 1H), 2.90 (s, 3H). ^{13}C NMR (101 MHz, DMSO-d_6) δ 171.77, 168.42, 140.32, 139.40, 138.59, 133.83, 132.00, 129.52, 129.49, 128.78, 128.68, 126.58, 126.45, 121.92, 119.54, 101.43, 43.54. HRMS (ES): calcd for $C_{17}H_{13}ClN_2O_4S$ $[M+H]^+$: 377.0363. Found: 377.0352.

3-(2-methoxyphenyl)-4-((3-(methylsulfonyl)phenyl)amino)-1H-pyrrole-2,5-dione (19).

Compound **19** was isolated as a yellow solid in 49% yield. ^{1}H NMR (400 MHz, DMSO-d_6) δ 10.79 (s, 1H), 9.70 (s, 1H), 7.38 – 7.33 (m, 1H), 7.30 (dd, *J* = 7.6, 1.7 Hz, 1H), 7.23 – 7.13 (m, 3H), 7.04 (ddd, *J* = 8.1, 2.2, 1.0 Hz, 1H), 6.93 (td, *J* = 7.5, 1.0 Hz, 1H), 6.54 (d, *J* = 8.4 Hz, 1H), 3.13 (s, 3H), 2.82 (s, 3H). ^{13}C NMR (101 MHz, DMSO-d_6) δ 172.53, 169.01, 156.28, 140.11, 139.12, 137.66, 130.55, 129.40, 128.48, 124.99, 120.79, 119.57, 119.00, 117.93, 109.84, 100.54, 54.43, 43.46. HRMS (ES): calcd for $C_{18}H_{16}N_2O_5S$ $[M+H]^+$: 373.0858. Found: 373.0843.

3-((3-hydroxyphenyl)amino)-4-(2-(trifluoromethyl)phenyl)-1H-pyrrole-2,5-dione (20).

Compound **20** was isolated as a yellow solid in 25% yield. ^{1}H NMR (400 MHz, DMSO-d_6) δ 10.74 (s, 1H), 9.26 (s, 1H), 9.16 (s, 1H), 7.51 (d, *J* = 8.1 Hz, 1H), 7.45 (t, *J* = 7.2 Hz, 1H), 7.37 (t, *J* = 7.6 Hz, 1H), 7.18 (d, *J* = 7.6 Hz, 1H), 6.56 (t, *J* = 8.0 Hz, 1H), 6.30 (t, *J* = 2.1 Hz, 1H), 6.22 (dd, *J* = 8.1, 2.3 Hz, 1H), 6.08 (dd, *J* = 7.3, 1.3 Hz, 1H). ^{13}C NMR (101 MHz, DMSO-d_6) δ 172.36, 168.62, 156.92, 140.57, 138.34, 132.91, 131.43, 129.76 (dd, *J* = 4.4, 2.3 Hz), 128.59, 128.31, 128.07, 128.00, 125.62 (d, *J* = 5.1 Hz), 125.30, 122.58, 113.60, 111.44, 110.24, 99.09. HRMS (ES): calcd for $C_{17}H_{11}F_3N_2O_3$ $[M+H]^+$: 349.0800. Found: 349.0786.

3-(2-chlorophenyl)-4-((3-hydroxyphenyl)amino)-1*H*-pyrrole-2,5-dione (21).

Compound **21** was isolated as a yellow solid in 67% yield. ^{1}H NMR (400 MHz, DMSO-d_6) δ 10.74 (s, 1H), 9.44 (s, 1H), 9.16 (s, 1H), 7.21 – 7.12 (m, 3H), 7.11 – 7.06 (m, 1H), 6.56 (t, *J* = 8.0 Hz, 1H), 6.32 (t, *J* = 2.2 Hz,

1H), 6.24 (dd, *J* = 8.1, 2.3 Hz, 1H), 6.01 (dd, *J* = 8.0, 2.0 Hz, 1H). ^{13}C NMR (101 MHz, DMSO-d_6) δ 171.95, 168.64, 156.83, 140.00, 138.38, 133.95, 131.92, 130.22, 129.02, 128.38, 127.75, 126.16, 112.70, 111.11, 109.51, 99.58. HRMS (ES): calcd for $C_{16}H_{11}ClN_2O_3$ $[M+H]^+$: 315.0536. Found: 315.0524.

3-((4-hydroxyphenyl)amino)-4-(2-(trifluoromethyl)phenyl)-1H-pyrrole-2,5-dione (22).

Compound **22** was isolated as a yellow solid in 41% yield. ^{1}H NMR (400 MHz, DMSO-d_6) δ 10.64 (s, 1H), 9.16 (s, 1H), 9.12 (s, 1H), 7.48 (d, *J* = 7.7 Hz, 1H), 7.39 (dt, *J* = 23.9, 7.5 Hz, 2H), 7.15 (d, *J* = 7.4 Hz, 1H), 6.62 – 6.55 (m, 2H), 6.28 – 6.22 (m, 2H). ^{13}C NMR (101 MHz, dmso) δ 172.39, 168.57, 154.36, 141.52, 133.34, 131.30, 129.84 (q, *J* = 2.1 Hz), 128.81, 128.53, 128.46, 127.92, 125.53 (q, *J* = 4.9 Hz), 125.28, 124.94, 122.56, 114.12, 97.09. HRMS (ES): calcd for $C_{17}H_{11}F_3N_2O_3$ $[M+H]^+$: 349.0800. Found: 349.0787.

3-(2-chlorophenyl)-4-((4-hydroxyphenyl)amino)-1H-pyrrole-2,5-dione (23).

Compound **23** was isolated as an orange solid in 73% yield. ^{1}H NMR (400 MHz, DMSO-d_6) δ 10.64 (s, 1H), 9.34 (s, 1H), 9.11 (s, 1H), 7.14 (ddt, *J* = 8.8, 5.1, 2.5 Hz, 3H), 7.06 – 7.02 (m, 1H), 6.56 (d, *J* = 8.8 Hz, 2H), 6.26 (d, *J* = 8.8 Hz, 2H). ^{13}C NMR (101 MHz, DMSO-d_6) δ 171.98, 168.57, 154.07, 140.84, 134.05, 132.20, 130.29, 128.87, 128.56, 128.31, 126.05, 123.88, 113.91, 97.48. HRMS (ES): calcd for $C_{16}H_{11}ClN_2O_3$ $[M+H]^+$: 315.0536. Found: 315.0525.

3-((4-hydroxyphenyl)amino)-4-(2-methoxyphenyl)-1H-pyrrole-2,5-dione (24).

Compound **24** was isolated as an orange solid in 64% yield. ^{1}H NMR (400 MHz, DMSO-d_6) δ 10.52 (s, 1H), 9.10 (s, 1H), 9.02 (s, 1H), 7.17 – 7.10 (m, 2H), 6.85 (td, *J* = 7.5, 1.0 Hz, 1H), 6.55 – 6.47 (m, 3H), 6.29 – 6.24 (m, 2H), 3.17 (s, 3H). ^{13}C NMR (101 MHz, DMSO-d_6) δ 172.79, 169.17, 156.65, 153.38, 139.23, 130.42, 129.36, 128.65, 122.42, 119.86, 119.22, 113.60, 109.80, 96.40, 54.44. HRMS (ES): calcd for $C_{17}H_{14}N_2O_4$ $[M+H]^+$: 311.1032. Found: 311.1021.

3-((3-fluorophenyl)amino)-4-(2-(trifluoromethyl)phenyl)-1H-pyrrole-2,5-dione (25).

Compound **25** was isolated as a yellow solid in 22% yield. ^{1}H NMR (400 MHz, DMSO-d_6) δ 10.87 (s, 1H), 9.54 (s, 1H), 7.58 – 7.48 (m, 2H), 7.42 (t, *J* = 7.6 Hz, 1H), 7.28 (d, *J* = 7.6 Hz, 1H), 6.92 (td, *J* = 8.2, 6.8 Hz, 1H), 6.65 (dd, *J* = 11.2, 5.6 Hz, 2H), 6.52 (dt, *J* = 10.8, 2.2 Hz, 1H). ^{13}C NMR (101 MHz, DMSO-d_6) δ 172.25, 168.52, 162.54, 160.13, 140.07, 139.44, 139.34, 132.67, 131.72, 129.55 (d, *J* = 2.2 Hz), 129.28, 129.18, 128.63, 128.47, 128.34, 128.05, 127.92, 125.78 (q, *J* = 5.1 Hz), 125.20, 122.47, 118.51 (d, *J* = 2.7 Hz), 110.71, 110.50, 109.64, 109.40, 100.48. HRMS (ES): calcd for $C_{17}H_{10}F_4N_2O_2$ $[M+H]^+$: 351.0757 .Found: 351.0746.

3-(2-chlorophenyl)-4-((3-fluorophenyl)amino)-1*H*-pyrrole-2,5-dione (26).

Compound **26** was isolated as a yellow solid in 61% yield. ^{1}H NMR (400 MHz, DMSO-d_6) δ 10.84 (s, 1H), 9.69 (s, 1H), 7.22 – 7.12 (m, 4H), 6.89 (td, *J* = 8.2, 6.7 Hz, 1H), 6.62 (td, *J* = 8.6, 2.5 Hz, 1H), 6.57 (dd, *J* = 8.1,

2.0 Hz, 1H), 6.44 (dt, *J* = 11.0, 2.3 Hz, 1H). ^{13}C NMR (101 MHz, DMSO-*d*$_6$) δ 171.85, 168.54, 162.49, 160.08, 139.49, 139.41, 139.31, 133.92, 131.83, 129.99, 129.42, 128.98, 128.89, 128.49, 126.42, 117.73 (d, *J* = 2.7 Hz), 110.28, 110.07, 108.80, 108.55, 100.94. HRMS (ES): calcd for $C_{16}H_{10}ClFN_2O_2$ $[M+H]^+$: 317.0493. Found: 317.0484.

3-((3-fluorophenyl)amino)-4-(2-methoxyphenyl)-1H-pyrrole-2,5-dione (27).

Compound **27** was isolated as a yellow solid in 77% yield. ^{1}H NMR (400 MHz, DMSO-*d*$_6$) δ 10.74 (s, 1H), 9.51 (s, 1H), 7.26 (dd, *J* = 7.6, 1.7 Hz, 1H), 7.20 (ddd, *J* = 8.4, 7.4, 1.8 Hz, 1H), 6.97 – 6.89 (m, 2H), 6.62 (td, *J* = 8.6, 2.5 Hz, 1H), 6.56 (ddd, *J* = 8.2, 2.9, 1.1 Hz, 2H), 6.36 (dt, *J* = 11.3, 2.3 Hz, 1H), 3.13 (s, 3H). ^{13}C NMR (101 MHz, dmso) δ 172.63, 169.12, 162.53, 160.13, 156.52, 140.03, 139.92, 137.73, 130.28, 129.28, 128.66, 128.57, 119.48, 119.41, 116.40 (d, *J* = 2.6 Hz), 109.78, 109.19, 108.98, 107.32, 107.07, 100.13, 54.40. HRMS (ES): calcd for $C_{17}H_{13}FN_2O_3$ $[M+H]^+$: 313.0988. Found: 313.0978.

3-(2-chlorophenyl)-4-((3-(trifluoromethyl)phenyl)amino)-1H-pyrrole-2,5-dione (28).

Compound **28** was isolated as a yellow solid in 29% yield. ^{1}H NMR (400 MHz, DMSO-*d*$_6$) δ 10.90 (s, 1H), 9.84 (s, 1H), 7.24 – 7.14 (m, 7H), 6.87 (s, 1H). ^{13}C NMR (101 MHz, DMSO-*d*$_6$) δ 171.81, 168.50, 139.32, 138.36, 133.74, 131.80, 129.61, 129.44, 128.82, 128.57, 128.23, 127.91, 127.64, 126.44, 125.50, 124.93, 122.22, 119.99 (q, *J* = 3.5 Hz), 117.51 (q, *J* = 4.0 Hz), 101.11. HRMS (ES): calcd for $C_{17}H_{10}ClF_3N_2O_2$ $[M+H]^+$: 367.0461. Found: 367.0451.

3-(2-methoxyphenyl)-4-((3-(trifluoromethyl)phenyl)amino)-1H-pyrrole-2,5-dione (29).

Compound **29** was isolated as a yellow solid in 51% yield. ^{1}H NMR (400 MHz, DMSO-*d*$_6$) δ 10.77 (s, 1H), 9.64 (s, 1H), 7.26 (dd, *J* = 7.6, 1.7 Hz, 1H), 7.21 – 7.10 (m, 3H), 7.07 (d, *J* = 7.9 Hz, 1H), 6.91 (td, *J* = 7.5, 1.0 Hz, 1H), 6.81 (s, 1H), 6.50 (d, *J* = 8.4 Hz, 1H), 3.08 (s, 3H). ^{13}C NMR (101 MHz, dmso) δ 172.58, 169.08, 156.19, 138.85, 137.67, 130.25, 129.35, 128.72, 128.38 (d, *J* = 4.0 Hz), 128.09, 127.77, 125.05, 124.04, 122.34, 119.50, 119.03, 118.92 (dd, *J* = 7.5, 3.7 Hz), 116.21 (q, *J* = 3.9 Hz), 109.71, 100.27, 54.26. HRMS (ES): calcd for $C_{18}H_{13}F_3N_2O_3$ $[M+H]^+$: 363.0957. Found: 363.0945.

3-((3-chlorophenyl)amino)-4-(2-(trifluoromethyl)phenyl)-1H-pyrrole-2,5-dione (30).

Compound **30** was isolated as a yellow solid in 21% yield. ^{1}H NMR (400 MHz, DMSO-*d*$_6$) δ 10.87 (s, 1H), 9.54 (s, 1H), 7.53 (dd, *J* = 14.4, 7.5 Hz, 2H), 7.42 (t, *J* = 7.6 Hz, 1H), 7.27 (d, *J* = 7.6 Hz, 1H), 6.95 (t, *J* = 8.0 Hz, 1H), 6.86 (ddd, *J* = 8.0, 2.0, 1.1 Hz, 1H), 6.81 (ddd, *J* = 8.0, 2.0, 1.0 Hz, 1H), 6.73 (t, *J* = 2.0 Hz, 1H). ^{13}C NMR (101 MHz, DMSO-*d*$_6$) δ 172.21, 168.49, 140.00, 139.02, 132.60, 132.21, 131.79, 129.45 (q, *J* = 2.3 Hz), 129.30, 128.52 (d, *J* = 3.2 Hz), 128.25, 127.94 (d, *J* = 2.6 Hz), 125.86 (q, *J* = 5.0 Hz), 125.21, 123.78, 122.48, 122.33, 121.10, 100.49. HRMS (ES): calcd for $C_{17}H_{10}ClF_3N_2O_2$ $[M+H]^+$: 367.0461. Found: 367.0451.

3-((3-chlorophenyl)amino)-4-(2-methoxyphenyl)-1H-pyrrole-2,5-dione (31).

Compound **31** was isolated as a yellow solid in 68% yield. ^{1}H NMR (400 MHz, DMSO-d_6) δ 10.74 (s, 1H), 9.50 (s, 1H), 7.26 – 7.22 (m, 1H), 7.22 – 7.18 (m, 1H), 6.96 – 6.89 (m, 2H), 6.84 (ddd, *J* = 8.0, 2.0, 1.0 Hz, 1H), 6.70 (ddd, *J* = 8.1, 2.1, 1.0 Hz, 1H), 6.62 – 6.56 (m, 2H), 3.15 (s, 3H). ^{13}C NMR (101 MHz, DMSO-d_6) δ 172.59, 169.08, 156.37, 139.55, 137.73, 131.99, 130.25, 129.39, 128.66, 122.26, 120.14, 119.54, 119.32, 119.00, 109.84, 100.17, 54.39. HRMS (ES): calcd for $C_{17}H_{13}ClN_2O_3$ $[M+H]^+$: 329.0693. Found: 329.0683.

3-((3-chloro-4-hydroxyphenyl)amino)-4-(2-(trifluoromethyl)phenyl)-1H-pyrrole-2,5-dione (32)

Compound **32** was isolated as a green solid in 40% yield. ^{1}H NMR (400 MHz, DMSO-d_6) δ 10.71 (s, 1H), 9.85 (s, 1H), 9.25 (s, 1H), 7.53 (d, *J* = 8.2 Hz, 1H), 7.47 (t, *J* = 7.2 Hz, 1H), 7.39 (t, *J* = 7.6 Hz, 1H), 7.20 (d, *J* = 7.6 Hz, 1H), 6.69 (d, *J* = 2.6 Hz, 1H), 6.62 (dd, *J* = 8.7, 2.6 Hz, 1H), 6.49 (d, *J* = 8.7 Hz, 1H). ^{13}C NMR (101 MHz, DMSO-d_6) δ 172.29, 168.47, 150.00, 141.08, 132.99, 131.48, 129.61 (d, *J* = 2.2 Hz), 129.36, 128.65, 128.36, 128.17, 125.67 (q, *J* = 4.9 Hz), 125.26, 125.12, 123.34, 122.54, 118.41, 115.33, 98.13. HRMS (ES): calcd for $C_{17}H_{10}ClF_3N_2O_3$ $[M+H]^+$: 383.0410. Found: 383.0396.

3-((3-chloro-4-hydroxyphenyl)amino)-4-(2-chlorophenyl)-1H-pyrrole-2,5-dione (33).

Compound **33** was isolated as an orange solid in 62% yield. ^{1}H NMR (400 MHz, DMSO-d_6) δ 10.72 (s, 1H), 9.83 (s, 1H), 9.43 (s, 1H), 7.23 – 7.14 (m, 3H), 7.12 – 7.08 (m, 1H), 6.67 (d, *J* = 2.6 Hz, 1H), 6.58 (dd, *J* = 8.8, 2.6 Hz, 1H), 6.49 (d, *J* = 8.7 Hz, 1H). ^{13}C NMR (101 MHz, DMSO-d_6) δ 171.91, 168.49, 149.68, 140.40, 133.92, 131.97, 130.09, 129.49, 129.18, 128.48, 126.28, 124.07, 122.33, 118.36, 115.10, 98.57. HRMS (ES): calcd for $C_{16}H_{10}Cl_2N_2O_3$ $[M+H]^+$: 349.0147. Found: 349.0135.

3-((3,5-dichloro-4-hydroxyphenyl)amino)-4-(2-(trifluoromethyl)phenyl)-1H-pyrrole-2,5-dione (34).

Compound **34** was isolated as a brown solid in 23% yield. ^{1}H NMR (400 MHz, DMSO-d_6) δ 10.81 (s, 1H), 9.81 (s, 1H), 9.35 (s, 1H), 7.60 – 7.49 (m, 2H), 7.42 (t, *J* = 7.7 Hz, 1H), 7.26 (d, *J* = 7.6 Hz, 1H), 6.77 (s, 2H). ^{13}C NMR (101 MHz, DMSO-d_6) δ 172.18, 168.38, 145.75, 140.49, 132.73, 131.70, 130.19, 129.39 (d, *J* = 2.2 Hz), 128.53, 128.45, 128.24, 127.96, 125.84 (q, *J* = 5.2 Hz), 125.24, 123.43, 122.52, 121.28, 99.42. HRMS (ES): calcd for $C_{17}H_9Cl_2F_3N_2O_3$ $[M+H]^+$: 417.0021. Found: 417.0009.

3-(2-chlorophenyl)-4-((3,5-dichloro-4-hydroxyphenyl)amino)-1H-pyrrole-2,5-dione (35).

Compound **35** was isolated as a yellow solid in 51% yield. ^{1}H NMR (400 MHz, DMSO-d_6) δ 10.81 (s, 1H), 9.77 (s, 1H), 9.53 (s, 1H), 7.29 – 7.25 (m, 1H), 7.25 – 7.20 (m, 2H), 7.20 – 7.15 (m, 1H), 6.74 (s, 2H). ^{13}C NMR (101 MHz, DMSO-d_6) δ 171.81, 168.40, 145.38, 139.83, 133.82, 131.82, 130.32, 129.90, 129.50, 128.63, 126.51, 122.45, 121.21, 99.89. HRMS (ES): calcd for $C_{16}H_9Cl_3N_2O_3$ $[M+H]^+$: 382.9757. Found: 382.9746.

3-((3,5-dichloro-4-hydroxyphenyl)amino)-4-(2-methoxyphenyl)-1H-pyrrole-2,5-dione (36).

Compound **36** was isolated as a yellow solid in 64% yield. ^{1}H NMR (400 MHz, DMSO-d_6) δ 10.64 (s, 1H), 9.60 (s, 1H), 9.28 (s, 1H), 7.16 (ddt, *J* = 7.6, 4.5, 1.5 Hz, 2H), 6.86 (td, *J* = 7.5, 1.0 Hz, 1H), 6.64 (s, 2H), 6.61 (d, *J* = 8.1 Hz, 1H), 3.23 (s, 3H). ^{13}C NMR (101 MHz, DMSO-d_6) δ 172.54, 168.96, 156.34, 144.56, 138.31, 131.01, 130.32, 129.40, 121.23, 121.09, 119.64, 119.25, 109.87, 99.10, 54.48. HRMS (ES): calcd for $C_{17}H_{12}Cl_2N_2O_4$ $[M+H]^+$: 379.0252. Found: 379.0241.

3-((3-chloro-4-methoxybenzyl)amino)-4-(2-(trifluoromethyl)phenyl)-1H-pyrrole-2,5-dione (37).

Compound **37** was isolated as a beige solid in 30% yield. ^{1}H NMR (400 MHz, DMSO-d_6) δ 10.54 (s, 1H), 7.96 (t, *J* = 6.6 Hz, 1H), 7.70 (d, *J* = 7.6 Hz, 1H), 7.60 – 7.48 (m, 2H), 7.13 (d, *J* = 7.0 Hz, 1H), 6.94 (d, *J* = 8.5 Hz, 1H), 6.75 – 6.58 (m, 2H), 3.96 (dd, *J* = 15.1, 5.4 Hz, 1H), 3.79 (s, 3H). ^{13}C NMR (101 MHz, dmso) δ 172.13, 168.21, 153.46, 143.43, 134.13, 131.47, 131.19, 130.12, 129.83, 129.46 (d, *J* = 2.0 Hz), 128.53, 127.97, 126.32, 125.81 (dd, *J* = 10.0, 5.2 Hz), 125.28, 122.55, 120.57, 112.48, 56.06, 44.86. HRMS (ES): calcd for $C_{19}H_{14}ClF_3N_2O_3$ $[M+H]^+$: 411.0723. Found: 411.0711.

3-((3-chloro-4-methoxybenzyl)amino)-4-(2-chlorophenyl)-1H-pyrrole-2,5-dione (38).

Compound **38** was isolated as a beige solid in 56% yield. ^{1}H NMR (400 MHz, DMSO-d_6) δ 10.53 (s, 1H), 8.05 (t, *J* = 6.7 Hz, 1H), 7.40 (dd, *J* = 8.0, 1.2 Hz, 1H), 7.35 (td, *J* = 7.6, 1.7 Hz, 1H), 7.25 (td, *J* = 7.4, 1.4 Hz, 1H), 7.13 (dd, *J* = 7.6, 1.6 Hz, 1H), 6.92 (d, *J* = 8.5 Hz, 1H), 6.68 (d, *J* = 8.0 Hz, 1H), 6.59 (s, 1H), 4.01 (t, *J* = 6.7 Hz, 2H), 3.78 (s, 3H). ^{13}C NMR (101 MHz, DMSO-d_6) δ 171.75, 168.27, 153.42, 143.32, 135.25, 133.57, 131.36, 129.89, 129.44, 128.68, 128.00, 126.39, 126.20, 120.54, 112.53, 56.06, 44.82. HRMS (ES): calcd for $C_{18}H_{14}Cl_2N_2O_3$ $[M+H]^+$: 377.0460. Found: 377.0448.

3-((3-chloro-4-methoxybenzyl)amino)-4-(2-methoxyphenyl)-1H-pyrrole-2,5-dione (39).

Compound **39** was isolated as a beige solid in 52% yield. ^{1}H NMR (400 MHz, DMSO-d_6) δ 10.36 (s, 1H), 7.70 (s, 1H), 7.31 (ddd, *J* = 8.3, 7.4, 1.8 Hz, 1H), 6.99 (dd, *J* = 7.4, 1.5 Hz, 1H), 6.96 – 6.86 (m, 3H), 6.76 – 6.61 (m, 2H), 4.03 (s, 2H), 3.78 (s, 3H), 3.61 (s, 3H). ^{13}C NMR (101 MHz, DMSO-d_6) δ 172.42 (s), 168.73, 157.73, 153.29, 143.05, 132.53, 131.97, 129.06, 128.28, 126.63, 120.40, 119.46, 119.26, 112.37, 110.53, 56.02, 54.95, 44.43. HRMS (ES): calcd for $C_{19}H_{17}ClN_2O_4$ $[M+H]^+$: 373.0955. Found: 373.0945.

3-((4-(2-chlorophenyl)-2,5-dioxo-2,5-dihydro-1H-pyrrol-3-yl)amino)benzonitrile (40).

Compound **40** was isolated as a yellow solid in 56% yield. ^{1}H NMR (400 MHz, DMSO-d_6) δ 10.91 (s, 1H), 9.87 (s, 1H), 7.29 – 7.22 (m, 4H), 7.18 (td, *J* = 5.6, 3.2 Hz, 3H), 6.91 (dd, *J* = 3.1, 1.1 Hz, 1H). ^{13}C NMR (101 MHz, DMSO-d_6) δ 171.77, 168.45, 139.45, 138.32, 133.75, 131.73, 129.73, 129.67, 128.89, 128.57, 126.99, 126.67,

126.55, 124.55, 117.91, 110.24, 101.35. HRMS (ES): calcd for $C_{17}H_{10}ClN_3O_2$ $[M+H]^+$: 324.0540. Found: 324.0531.

3-((4-(2-methoxyphenyl)-2,5-dioxo-2,5-dihydro-1H-pyrrol-3-yl)amino)benzonitrile (41).

Compound **41** was isolated as a yellow solid in 54% yield. ^{1}H NMR (400 MHz, DMSO-d_6) δ 10.78 (s, 1H), 9.66 (s, 1H), 7.31 – 7.19 (m, 3H), 7.15 (t, *J* = 7.8 Hz, 1H), 7.13 – 7.07 (m, 1H), 6.94 (td, *J* = 7.5, 0.9 Hz, 1H), 6.80 (t, *J* = 1.7 Hz, 1H), 6.54 (d, *J* = 7.9 Hz, 1H), 3.13 (s, 3H). ^{13}C NMR (101 MHz, DMSO-d_6) δ 172.49, 169.02, 156.16, 138.83, 137.69, 130.26, 129.60, 128.56, 125.96, 125.14, 123.02, 119.69, 119.11, 118.16, 110.06, 109.79, 100.65, 54.39. HRMS (ES): calcd for $C_{18}H_{13}N_3O_3$ $[M+H]^+$: 320.1035. Found: 320.1022.

3-((2,5-dioxo-4-(2-phenoxyphenyl)-2,5-dihydro-1H-pyrrol-3-yl)amino)benzonitrile (42).

Compound **42** was isolated as a yellow solid in 78% yield. ^{1}H NMR (400 MHz, DMSO-d_6); mixture of rotamers: δ 10.82 – 10.66 (m, 1H), 9.92 – 9.72 (m, 1H), 7.53 – 7.34 (m, 2H), 7.27 (m, 5H), 7.20 – 7.14 (m, 1H), 7.08 – 7.00 (m, 1H), 6.96 (s, 1H), 6.51 (m, 3H). ^{13}C NMR (126 MHz, DMSO-d_6); mixture of rotamers; δ 172.51, 172.24, 169.09, 168.79, 156.37, 155.91, 154.27, 153.73, 139.54, 139.41, 138.64, 133.87, 132.77, 132.71, 131.79, 131.68, 130.23, 130.20, 130.05, 129.58, 129.41, 127.15, 126.72, 126.28, 125.87, 124.73, 124.69, 124.35, 124.31, 124.02, 123.82, 123.67, 123.58, 122.62, 119.97, 119.51, 118.94, 118.64, 118.54, 118.19, 118.07, 117.89, 115.26, 114.88, 110.97, 110.86, 100.91, 99.18. HRMS (ES): calcd for $C_{23}H_{15}N_3O_3$ $[M+H]^+$: 382.1192. Found: 382.1202.

3-((2,5-dioxo-4-(4-phenoxyphenyl)-2,5-dihydro-1H-pyrrol-3-yl)amino)benzonitrile (43).

Compound **43** was isolated as a yellow solid in 29% yield. ^{1}H NMR (400 MHz, DMSO-d_6) δ 10.84 (s, 1H), 9.70 (s, 1H), 7.41 – 7.35 (m, 3H), 7.30 (t, *J* = 7.9 Hz, 1H), 7.21 (ddd, *J* = 8.2, 2.1, 1.2 Hz, 1H), 7.13 (ddd, *J* = 10.3, 2.4, 1.4 Hz, 1H), 6.96 (ddd, *J* = 9.5, 3.7, 1.9 Hz, 4H), 6.90 – 6.86 (m, 1H), 6.80 – 6.74 (m, 2H). ^{13}C NMR (126 MHz, DMSO-d_6) δ 172.61, 169.00, 156.71, 155.57, 138.57, 136.82, 130.99, 130.00, 129.25, 126.38, 125.97, 125.04, 124.23, 123.40, 118.35, 118.29, 117.76, 110.45, 104.63. HRMS (ES): calcd for $C_{23}H_{15}N_3O_3$ $[M+H]^+$: 382.1192. Found: 382.1202.

3-((4-(naphthalen-1-yl)-2,5-dioxo-2,5-dihydro-1H-pyrrol-3-yl)amino)benzonitrile (44).

Compound **44** was isolated as a yellow solid in 22% yield. ^{1}H NMR (500 MHz, DMSO-d_6) δ 10.86 (s, 1H), 9.72 (s, 1H), 7.80 – 7.73 (m, 2H), 7.60 – 7.55 (m, 1H), 7.41 – 7.32 (m, 3H), 7.24 (d, *J* = 7.1 Hz, 1H), 6.97 – 6.92 (m, 2H), 6.80 (t, *J* = 7.9 Hz, 1H), 6.74 – 6.71 (m, 1H). ^{13}C NMR (126 MHz, DMSO-d_6) δ 172.68, 168.80, 139.73, 138.46, 132.76, 131.34, 128.25, 128.17, 128.08, 127.88, 126.37, 125.93, 125.58, 125.36, 124.98, 124.16, 117.72, 109.74, 102.87. HRMS (ES): calcd for $C_{21}H_{13}N_3O_2$ $[M+H]^+$: 340.1086. Found: 340.1079.

3-(2-methoxyphenyl)-4-((2-methoxyphenyl)amino)-1H-pyrrole-2,5-dione (45).

Compound **45** was isolated as a yellow solid in 48% yield. ^{1}H NMR (400 MHz, DMSO-d_6) δ 10.62 (s, 1H), 8.21 (s, 1H), 7.15 – 7.11 (m, 1H), 7.11 – 7.07 (m, 1H), 6.91 – 6.79 (m, 2H), 6.75 (d, *J* = 8.1 Hz, 1H), 6.50 (d, *J* = 8.3 Hz, 1H), 6.40 (d, *J* = 4.6 Hz, 2H), 3.69 (s, 3H), 3.18 (s, 3H). ^{13}C NMR (101 MHz, DMSO-d_6) δ 172.61, 169.06, 156.54, 151.27, 138.66, 130.54, 128.70, 126.25, 124.97, 122.21, 119.03, 118.99, 118.63, 110.21, 109.64, 98.41, 55.28, 54.13. HRMS (ES): calcd for $C_{18}H_{16}N_2O_4$ $[M+H]^+$: 325.1188. Found: 325.1176.

3-(2-methoxyphenyl)-4-((3-methoxyphenyl)amino)-1H-pyrrole-2,5-dione (46).

Compound **46** was isolated as a yellow solid in 70% yield. ^{1}H NMR (400 MHz, DMSO-d_6) δ 10.70 (s, 1H), 9.34 (s, 1H), 7.28 (dd, *J* = 7.6, 1.7 Hz, 1H), 7.19 (ddd, *J* = 8.3, 7.4, 1.8 Hz, 1H), 6.94 – 6.85 (m, 2H), 6.56 (d, *J* = 8.4 Hz, 1H), 6.51 – 6.46 (m, 1H), 6.38 (dd, *J* = 8.2, 2.5 Hz, 1H), 6.07 (t, *J* = 2.2 Hz, 1H), 3.22 (s, 3H), 3.07 (s, 3H). ^{13}C NMR (101 MHz, DMSO-d_6) δ 172.81, 169.21, 158.45, 156.76, 139.41, 137.83, 130.48, 128.98, 128.03, 119.79, 119.23, 113.00, 109.85, 109.69, 104.89, 98.71, 54.35, 54.32. HRMS (ES): calcd for $C_{18}H_{16}N_2O_4$ $[M+H]^+$: 325.1188. Found: 325.1178.

3-(2-methoxyphenyl)-4-((4-methoxyphenyl)amino)-1H-pyrrole-2,5-dione (47).

Compound **47** was isolated as an orange solid in 55% yield. ^{1}H NMR (400 MHz, DMSO-d_6) δ 10.56 (s, 1H), 9.21 (s, 1H), 7.18 – 7.12 (m, 2H), 6.86 (td, *J* = 7.5, 1.0 Hz, 1H), 6.63 – 6.57 (m, 2H), 6.51 (d, *J* = 8.0 Hz, 1H), 6.46 – 6.41 (m, 2H), 3.58 (s, 3H), 3.16 (s, 3H). ^{13}C NMR (101 MHz, DMSO-d_6) δ 172.75, 169.15, 156.54, 155.29, 139.09, 130.87, 130.36, 128.70, 122.27, 119.74, 119.28, 112.37, 109.79, 97.03, 55.17, 54.42. HRMS (ES): calcd for $C_{18}H_{16}N_2O_4$ $[M+H]^+$: 325.1188. Found: 325.1178.

3-((2,4-dimethoxyphenyl)amino)-4-(2-methoxyphenyl)-1H-pyrrole-2,5-dione (48).

Compound **48** was isolated as an orange solid in 64% yield. ^{1}H NMR (400 MHz, DMSO-d_6) δ 10.48 (s, 1H), 8.24 (s, 1H), 7.09 (ddd, *J* = 8.3, 7.4, 1.8 Hz, 1H), 6.96 (dd, *J* = 7.5, 1.7 Hz, 1H), 6.76 (td, *J* = 7.4, 1.0 Hz, 1H), 6.51 (d, *J* = 8.3 Hz, 1H), 6.44 (d, *J* = 8.7 Hz, 1H), 6.23 (d, *J* = 2.6 Hz, 1H), 6.00 (dd, *J* = 8.6, 2.6 Hz, 1H), 3.61 (s, 3H), 3.60 (s, 3H), 3.29 (s, 3H). ^{13}C NMR (101 MHz, DMSO-d_6) δ 172.63, 169.01, 157.57, 156.58, 152.94, 140.05, 130.66, 128.39, 124.24, 119.33, 119.02, 118.86, 109.51, 102.82, 97.66, 97.27, 55.32, 55.18, 54.25. HRMS (ES): calcd for $C_{19}H_{18}N_2O_5$ $[M+H]^+$: 355.1294. Found: 355.1283.

3-((3,4-dimethoxyphenyl)amino)-4-(2-methoxyphenyl)-1H-pyrrole-2,5-dione (49).

Compound **49** was isolated as an orange solid in 70% yield. ^{1}H NMR (400 MHz, DMSO-d_6) δ 10.62 (s, 1H), 9.22 (s, 1H), 7.25 (dd, *J* = 7.5, 1.7 Hz, 1H), 7.17 (ddd, *J* = 8.3, 7.4, 1.8 Hz, 1H), 6.90 (td, *J* = 7.5, 1.0 Hz, 1H), 6.64 (d, *J* = 8.7 Hz, 1H), 6.58 – 6.50 (m, 2H), 6.05 (d, *J* = 2.5 Hz, 1H), 3.60 (s, 3H), 3.12 (s, 3H), 3.10 (s, 3H). ^{13}C NMR (101 MHz, DMSO-d_6) δ 172.84, 169.17, 156.83, 147.39, 144.75, 138.38, 131.72, 130.60, 128.80, 119.95,

119.16, 113.00, 111.18, 109.88, 105.14, 96.95, 55.76, 54.46, 54.40. HRMS (ES): calcd for $C_{19}H_{18}N_2O_5$ $[M+H]^+$: 355.1294. Found: 355.1280.

3-((3,5-dimethoxyphenyl)amino)-4-(2-methoxyphenyl)-1H-pyrrole-2,5-dione (50).

Compound **50** was isolated as a yellow solid in 61% yield. ^{1}H NMR (400 MHz, DMSO-*d*$_6$) δ 10.72 (s, 1H), 9.28 (s, 1H), 7.31 (dd, *J* = 7.6, 1.7 Hz, 1H), 7.21 (ddd, *J* = 8.3, 7.4, 1.8 Hz, 1H), 6.93 (td, *J* = 7.5, 1.0 Hz, 1H), 6.61 (d, *J* = 8.4 Hz, 1H), 5.97 (t, *J* = 2.2 Hz, 1H), 5.92 (d, *J* = 2.2 Hz, 2H), 3.31 (s, 6H), 3.11 (s, 3H). ^{13}C NMR (101 MHz, DMSO-*d*$_6$) δ 172.83, 169.21, 159.41, 156.99, 140.09, 137.58, 130.58, 129.00, 119.88, 119.18, 109.89, 99.02, 98.33, 96.16, 54.60, 54.46. HRMS (ES): calcd for $C_{19}H_{18}N_2O_5$ $[M+H]^+$: 355.1294. Found: 355.1283.

3-(benzo[d][1,3]dioxol-5-ylamino)-4-(2-methoxyphenyl)-1H-pyrrole-2,5-dione (51).

Compound **51** was isolated as an orange solid in 55% yield. ^{1}H NMR (400 MHz, DMSO-*d*$_6$) δ 10.59 (s, 1H), 9.21 (s, 1H), 7.20 – 7.11 (m, 2H), 6.86 (td, *J* = 7.5, 1.0 Hz, 1H), 6.59 (d, *J* = 8.4 Hz, 1H), 6.39 (d, *J* = 8.3 Hz, 1H), 6.31 (d, *J* = 2.1 Hz, 1H), 6.11 (dd, *J* = 8.4, 2.2 Hz, 1H), 5.81 (s, 2H), 3.23 (s, 3H). ^{13}C NMR (101 MHz, DMSO-*d*$_6$) δ 172.71, 169.12, 156.60, 146.18, 142.97, 138.95, 132.23, 130.33, 128.82, 119.69, 119.38, 114.14, 109.74, 106.41, 103.15, 100.75, 97.73, 54.52. HRMS (ES): calcd for $C_{18}H_{14}N_2O_5$ $[M+H]^+$: 339.0981. Found: 339.0970.

3-(2-methoxyphenyl)-4-((4-morpholinophenyl)amino)-1H-pyrrole-2,5-dione (52).

Compound **52** was isolated as a red solid in 47% yield. ^{1}H NMR (400 MHz, DMSO-*d*$_6$) δ 10.54 (s, 1H), 9.18 (s, 1H), 7.18 – 7.10 (m, 2H), 6.85 (td, *J* = 7.4, 1.0 Hz, 1H), 6.58 – 6.53 (m, 2H), 6.50 (d, *J* = 7.8 Hz, 1H), 6.47 – 6.42 (m, 2H), 3.70 – 3.62 (m, 4H), 3.14 (s, 3H), 2.92 – 2.83 (m, 4H). ^{13}C NMR (101 MHz, dmso) δ 172.73, 169.17, 156.56, 147.37, 139.01, 130.34, 129.98, 128.61, 121.79, 119.88, 119.24, 114.07, 109.85, 96.78, 65.92, 54.45, 49.07. HRMS (ES): calcd for $C_{21}H_{21}N_3O_4$ $[M+H]^+$: 380.1610. Found: 380.1594.

3-(2-methoxyphenyl)-4-(naphthalen-1-ylamino)-1H-pyrrole-2,5-dione (53).

Compound **53** was isolated as a brown solid in 58% yield. ^{1}H NMR (500 MHz, DMSO-*d*$_6$) δ 10.63 (s, 1H), 9.38 (s, 1H), 8.10 (d, *J* = 8.4 Hz, 1H), 7.81 (d, *J* = 8.1 Hz, 1H), 7.52 (s, 1H), 7.47 (dd, *J* = 12.3, 7.6 Hz, 2H), 7.02 – 6.92 (m, 2H), 6.81 (t, *J* = 7.8 Hz, 1H), 6.71 (t, *J* = 7.4 Hz, 1H), 6.53 (d, *J* = 7.3 Hz, 1H), 6.16 (d, *J* = 8.2 Hz, 1H), 2.58 (s, 3H). ^{13}C NMR (126 MHz, DMSO-*d*$_6$) δ 172.76, 169.03, 156.22, 140.66, 133.23, 133.05, 130.11, 128.46, 128.30, 127.60, 125.73, 125.45, 124.63, 123.86, 123.69, 120.31, 119.04, 118.99, 109.05, 98.25, 53.81. HRMS (ES): calcd for $C_{21}H_{16}N_2O_3$ $[M+H]^+$: 345.1239. Found: 345.1239.

3-([1,1'-biphenyl]-4-ylamino)-4-(2-methoxyphenyl)-1H-pyrrole-2,5-dione (54).

Compound **54** was isolated as an orange solid in 63% yield. ^{1}H NMR (500 MHz, DMSO-*d*$_6$) δ 10.69 (s, 1H), 9.48 (s, 1H), 7.47 (d, *J* = 7.4 Hz, 2H), 7.39 (t, *J* = 7.7 Hz, 2H), 7.31 – 7.22 (m, 2H), 7.18 (dd, *J* = 10.2, 5.0 Hz, 3H), 6.92 (t, *J* = 7.3 Hz, 1H), 6.74 (d, *J* = 8.5 Hz, 2H), 6.50 (d, *J* = 8.3 Hz, 1H), 3.11 (s, 3H). ^{13}C NMR (126 MHz, DMSO-

d$_6$) δ 172.72, 169.20, 156.66, 139.63, 138.23, 137.46, 134.53, 130.39, 128.98, 128.81, 126.93, 126.12, 125.23, 120.84, 119.69, 119.39, 109.81, 98.97, 54.41. HRMS (ES): calcd for $C_{23}H_{18}N_2O_3$ $[M+H]^+$: 371.1396. Found: 371.1413.

3-(benzo[d]thiazol-2-ylamino)-4-(2-methoxyphenyl)-1H-pyrrole-2,5-dione (55).

Compound **55** was isolated as a yellow solid in 57% yield. ^{1}H NMR (400 MHz, DMSO-*d*$_6$) δ 10.73 (s, 1H), 9.65 (s, 1H), 7.69 (d, *J* = 8.8 Hz, 1H), 7.27 (dd, *J* = 7.5, 1.5 Hz, 1H), 7.17 – 7.11 (m, 2H), 7.11 – 7.04 (m, 1H), 7.01 (d, *J* = 2.0 Hz, 1H), 6.89 (t, *J* = 7.4 Hz, 1H), 6.34 (d, *J* = 8.3 Hz, 1H), 3.00 (s, 3H). ^{13}C NMR (101 MHz, DMSO-*d*$_6$) δ 172.68, 169.15, 156.45, 154.24, 148.76, 138.22, 135.63, 132.89, 130.37, 129.21, 121.39, 120.50, 119.64, 119.22, 113.05, 109.63, 99.24, 54.38. HRMS (ES): calcd for $C_{18}H_{13}N_3O_3S$ $[M+H]^+$: 352.0756. Found: 352.0772.

3-((4-benzoylphenyl)amino)-4-(2-methoxyphenyl)-1H-pyrrole-2,5-dione (56).

Compound **56** was isolated as a yellow solid in 60% yield. ^{1}H NMR (400 MHz, DMSO-*d*$_6$) δ 10.82 (s, 1H), 9.82 (s, 1H), 7.67 – 7.61 (m, 1H), 7.59 – 7.50 (m, 4H), 7.29 (dd, *J* = 17.9, 8.1 Hz, 4H), 6.97 (t, *J* = 7.4 Hz, 1H), 6.76 (d, *J* = 8.6 Hz, 2H), 6.62 (d, *J* = 8.2 Hz, 1H), 3.13 (s, 3H). ^{13}C NMR (101 MHz, DMSO-*d*$_6$) δ 194.34, 172.51, 169.09, 156.64, 142.42, 137.45, 137.42, 132.22, 130.39, 130.37, 129.41, 129.36, 129.33, 128.33, 119.56, 119.40, 109.82, 101.83, 79.15, 54.56. HRMS (ES): calcd for $C_{24}H_{18}N_2O_4$ $[M+H]^+$: 399.1345. Found: 399.1362.

3-(2-methoxyphenyl)-4-((4-(phenylamino)phenyl)amino)-1H-pyrrole-2,5-dione (57).

Compound **57** was isolated as a red solid in 49% yield. ^{1}H NMR (500 MHz, DMSO-*d*$_6$) δ 10.55 (s, 1H), 9.23 (s, 1H), 7.88 (s, 1H), 7.18 (ddd, *J* = 13.1, 8.2, 3.6 Hz, 4H), 6.92 – 6.84 (m, 3H), 6.73 (t, *J* = 7.3 Hz, 1H), 6.63 – 6.55 (m, 5H), 3.22 (s, 3H). ^{13}C NMR (126 MHz, DMSO-*d*$_6$) δ 172.73, 169.17, 156.72, 144.04, 139.08, 138.59, 130.60, 130.44, 129.02, 128.68, 122.05, 119.97, 119.31, 118.89, 116.65, 115.52, 109.80, 96.87, 54.51. HRMS (ES): calcd for $C_{23}H_{19}N_3O_3$ $[M+H]^+$: 386.1505. Found: 386.1514.

3-(2-methoxyphenyl)-4-((3-(thiophen-3-yl)phenyl)amino)-1H-pyrrole-2,5-dione (58).

Compound **58** was isolated as a yellow solid in 52% yield. ^{1}H NMR (400 MHz, DMSO-*d*$_6$) δ 10.71 (s, 1H), 9.40 (s, 1H), 7.50 (dd, *J* = 5.0, 2.9 Hz, 1H), 7.34 (dd, *J* = 7.5, 1.6 Hz, 1H), 7.26 (d, *J* = 1.9 Hz, 1H), 7.16 (d, *J* = 7.7 Hz, 1H), 7.11 – 7.05 (m, 1H), 7.05 – 6.99 (m, 2H), 6.89 (t, *J* = 7.4 Hz, 1H), 6.84 (s, 1H), 6.80 (d, *J* = 7.9 Hz, 1H), 6.48 (d, *J* = 8.3 Hz, 1H), 3.07 (s, 3H). ^{13}C NMR (126 MHz, DMSO-*d*$_6$) δ 172.82, 169.24, 156.59, 140.97, 138.60, 137.97, 134.48, 130.44, 129.03, 127.86, 126.50, 126.01, 120.66, 119.70, 119.50, 119.28, 117.99, 109.92, 98.67, 54.33. HRMS (ES): calcd for $C_{21}H_{16}N_2O_3S$ $[M+H]^+$: 377.0960. Found: 377.0960.

3-(2-methoxyphenyl)-4-((4-(thiophen-3-yl)phenyl)amino)-1H-pyrrole-2,5-dione (59).

Compound **59** was isolated as an orange solid in 27% yield. ^{1}H NMR (400 MHz, DMSO-*d*$_6$) δ 10.69 (s, 1H), 9.43 (s, 1H), 7.66 (dd, *J* = 2.9, 1.3 Hz, 1H), 7.56 (dd, *J* = 5.0, 2.9 Hz, 1H), 7.39 (dd, *J* = 5.0, 1.3 Hz, 1H), 7.30 –

7.21 (m, 3H), 7.20 – 7.14 (m, 1H), 6.92 (t, *J* = 7.4 Hz, 1H), 6.69 (d, *J* = 8.6 Hz, 2H), 6.53 (d, *J* = 8.3 Hz, 1H), 3.11 (s, 3H). ^{13}C NMR (126 MHz, DMSO-*d*$_6$) δ 172.74, 169.21, 156.57, 140.94, 138.06, 137.07, 130.36, 129.69, 129.02, 126.88, 125.90, 124.75, 120.63, 119.76, 119.66, 119.44, 109.94, 98.88, 54.47. HRMS (ES): calcd for $C_{21}H_{16}N_2O_3S$ $[M+H]^+$: 377.0960. Found: 377.0960.

3-((3-(tert-butyl)phenyl)amino)-4-(2-methoxyphenyl)-1H-pyrrole-2,5-dione (60).

Compound **60** was isolated as a yellow solid in 65% yield. ^{1}H NMR (400 MHz, DMSO-*d*$_6$) δ 10.67 (s, 1H), 9.29 (s, 1H), 7.28 (dd, *J* = 7.6, 1.6 Hz, 1H), 7.18 – 7.12 (m, 1H), 6.91 (ddd, *J* = 9.3, 7.6, 4.5 Hz, 3H), 6.69 (d, *J* = 7.7 Hz, 1H), 6.55 (s, 1H), 6.50 (d, *J* = 8.2 Hz, 1H), 3.02 (s, 3H), 0.94 (s, 9H). ^{13}C NMR (126 MHz, DMSO-*d*$_6$) δ 172.87, 169.24, 156.61, 150.02, 138.03, 137.81, 130.59, 128.81, 127.03, 120.37, 119.59, 119.26, 118.00, 116.88, 109.87, 97.81, 54.26, 33.97, 30.74. HRMS (ES): calcd for $C_{21}H_{22}N_2O_3$ $[M+H]^+$: 351.1709. Found: 351.1726.

3-((3-(benzyloxy)phenyl)amino)-4-(2-methoxyphenyl)-1H-pyrrole-2,5-dione (61).

Compound **61** was isolated as a yellow solid in 65% yield. ^{1}H NMR (400 MHz, DMSO-*d*$_6$) δ 10.72 (s, 1H), 9.37 (s, 1H), 7.37 (t, *J* = 7.2 Hz, 2H), 7.32 (ddd, *J* = 7.1, 5.0, 2.2 Hz, 2H), 7.30 – 7.25 (m, 2H), 7.24 – 7.19 (m, 1H), 6.93 (dt, *J* = 11.3, 7.8 Hz, 2H), 6.56 (dd, *J* = 17.7, 8.1 Hz, 2H), 6.45 (dd, *J* = 8.1, 2.1 Hz, 1H), 6.12 (t, *J* = 2.0 Hz, 1H), 4.40 (s, 2H), 3.04 (s, 3H). ^{13}C NMR (126 MHz, DMSO-*d*$_6$) δ 172.80, 169.20, 157.63, 156.83, 139.41, 137.74, 136.83, 130.56, 129.05, 128.33, 128.12, 127.72, 127.49, 119.86, 119.25, 113.24, 110.12, 109.93, 105.79, 98.72, 68.49, 54.32. HRMS (ES): calcd for $C_{24}H_{20}N_2O_4$ $[M+H]^+$: 401.1501. Found: 401.1504.

3-((4-(benzyloxy)-3-chlorophenyl)amino)-4-(2-methoxyphenyl)-1H-pyrrole-2,5-dione (62).

Compound **62** was isolated as a yellow solid in 57% yield. ^{1}H NMR (400 MHz, DMSO-*d*$_6$) δ 10.64 (s, 1H), 9.32 (s, 1H), 7.44 – 7.30 (m, 5H), 7.15 (m, 2H), 6.87 (t, *J* = 7.4 Hz, 1H), 6.77 (d, *J* = 8.6 Hz, 1H), 6.66 – 6.61 (m, 2H), 6.44 (d, *J* = 8.2 Hz, 1H), 5.07 (s, 2H), 3.08 (s, 3H). ^{13}C NMR (126 MHz, DMSO-*d*$_6$) δ 172.64, 169.03, 156.34, 149.20, 138.50, 136.66, 131.97, 130.24, 129.10, 128.39, 127.81, 127.30, 122.61, 120.62, 119.46, 119.35, 113.52, 109.78, 98.27, 70.08, 54.29. HRMS (ES): calcd for $C_{24}H_{19}ClN_2O_4$ $[M+H]^+$: 435.1112. Found: 435.1122.

3-(2-methoxyphenyl)-4-(quinolin-6-ylamino)-1H-pyrrole-2,5-dione (63).

Compound **63** was isolated as a yellow solid in 36% yield. ^{1}H NMR (400 MHz, DMSO-*d*$_6$) δ 10.78 (s, 1H), 9.74 (s, 1H), 8.65 (dd, *J* = 4.2, 1.7 Hz, 1H), 7.69 (d, *J* = 9.0 Hz, 1H), 7.52 (dd, *J* = 9.1, 2.5 Hz, 1H), 7.43 (d, *J* = 8.4 Hz, 1H), 7.34 (dd, *J* = 7.5, 1.7 Hz, 1H), 7.29 (dd, *J* = 8.3, 4.2 Hz, 1H), 7.08 – 7.01 (m, 1H), 6.92 (t, *J* = 7.5 Hz, 1H), 6.55 (d, *J* = 2.4 Hz, 1H), 6.25 (d, *J* = 7.9 Hz, 1H), 2.94 (s, 3H). ^{13}C NMR (126 MHz, DMSO-*d*$_6$) δ 172.70, 169.22, 156.49, 148.70, 144.32, 137.78, 135.59, 134.47, 130.39, 129.27, 127.97, 127.16, 124.76, 121.42, 119.82, 119.08, 115.76, 109.65, 99.93, 54.40. HRMS (ES): calcd for $C_{20}H_{15}N_3O_3$ $[M+H]^+$: 346.1192. Found: 346.1207.

3-(2-methoxyphenyl)-4-(quinolin-8-ylamino)-1H-pyrrole-2,5-dione (64).

Compound **64** was isolated as a yellow solid in 42% yield. ^{1}H NMR (400 MHz, DMSO-d_6) δ 10.98 (s, 1H), 9.26 (s, 1H), 8.98 (dd, *J* = 4.2, 1.6 Hz, 1H), 8.38 (dd, *J* = 8.3, 1.6 Hz, 1H), 7.64 (dd, *J* = 8.3, 4.2 Hz, 1H), 7.49 (d, *J* = 8.2 Hz, 1H), 7.39 (dd, *J* = 7.6, 1.7 Hz, 1H), 7.33 – 7.27 (m, 1H), 7.01 (t, *J* = 7.1 Hz, 1H), 6.94 (t, *J* = 7.9 Hz, 1H), 6.62 (d, *J* = 8.2 Hz, 1H), 6.22 (d, *J* = 7.5 Hz, 1H), 2.72 (s, 3H). ^{13}C NMR (126 MHz, DMSO-d_6) δ 172.58, 169.31, 156.87, 149.33, 138.98, 136.51, 136.13, 133.49, 130.68, 129.64, 127.67, 125.40, 122.17, 121.48, 119.53, 119.22, 115.05, 110.14, 100.66, 54.02. HRMS (ES): calcd for $C_{20}H_{15}N_3O_3$ $[M+H]^+$: 346.1192. Found: 346.1176.

3-((4'-fluoro-[1,1'-biphenyl]-3-yl)amino)-4-(2-methoxyphenyl)-1H-pyrrole-2,5-dione (65).

Compound **65** was isolated as a yellow solid in 37% yield. ^{1}H NMR (400 MHz, DMSO-d_6) δ 10.73 (s, 1H), 9.45 (s, 1H), 7.33 (dd, *J* = 7.6, 1.7 Hz, 1H), 7.17 – 7.04 (m, 7H), 6.96 – 6.89 (m, 2H), 6.73 (s, 1H), 6.52 (d, *J* = 8.2 Hz, 1H), 3.07 (s, 3H). ^{13}C NMR (126 MHz, DMSO-d_6) δ 172.79, 169.23, 162.72, 160.77, 156.61, 138.73, 138.55, 137.87, 136.04 (d, *J* = 2.6 Hz), 130.58, 129.14, 128.87, 128.44, 128.37, 128.18, 128.06, 121.01, 119.80, 119.71, 119.26, 118.40, 115.30, 115.13, 109.98, 98.70, 54.36. HRMS (ES): calcd for $C_{23}H_{17}FN_2O_3$ $[M+H]^+$: 389.1301. Found: 389.1292.

3-((4-(3-methoxy-[1,1'-biphenyl]-4-yl)-2,5-dioxo-2,5-dihydro-1H-pyrrol-3-yl)amino)benzonitrile (66).

Compound **66** was isolated as a yellow solid in 52% yield. ^{1}H NMR (400 MHz, DMSO-d_6) δ 10.81 (s, 1H), 9.71 (s, 1H), 7.61 (dt, *J* = 7.9, 2.6 Hz, 2H), 7.45 (t, *J* = 7.5 Hz, 2H), 7.40 – 7.33 (m, 2H), 7.26 – 7.17 (m, 4H), 6.84 – 6.68 (m, 2H), 3.20 (s, 3H). ^{13}C NMR (126 MHz, DMSO-d_6) δ 172.51, 169.03, 156.53, 141.99, 140.25, 138.81, 137.76, 130.58, 128.78, 128.60, 128.27, 127.57, 126.92, 126.03, 125.29, 123.30, 122.96, 118.38, 110.02, 108.13, 100.34, 54.54. HRMS (ES): calcd for $C_{24}H_{17}N_3O_3$ $[M+H]^+$: 396.1348. Found: 396.1329.

3-((4-(4-methoxy-[1,1'-biphenyl]-3-yl)-2,5-dioxo-2,5-dihydro-1H-pyrrol-3-yl)amino)benzonitrile (67).

Compound **67** was isolated as a yellow solid in 45% yield. ^{1}H NMR (400 MHz, DMSO-d_6) δ 10.82 (s, 1H), 9.73 (s, 1H), 7.55 (dd, *J* = 8.2, 1.1 Hz, 2H), 7.50 (dd, *J* = 7.7, 2.1 Hz, 2H), 7.44 (t, *J* = 7.7 Hz, 2H), 7.35 – 7.29 (m, 1H), 7.26 – 7.17 (m, 3H), 6.85 (s, 1H), 6.64 (d, *J* = 9.3 Hz, 1H), 3.19 (s, 3H). ^{13}C NMR (126 MHz, DMSO-d_6) δ 172.52, 169.01, 155.87, 139.93, 138.80, 138.04, 131.98, 128.78, 128.71, 128.64, 127.85, 126.74, 126.42, 126.13, 125.44, 123.29, 119.56, 118.11, 110.33, 110.11, 100.45, 54.69. HRMS (ES): calcd for $C_{24}H_{17}N_3O_3$ $[M+H]^+$: 396.1348. Found: 396.1366.

3-((4-(4'-(benzyloxy)-3'-fluoro-3-methoxy-[1,1'-biphenyl]-4-yl)-2,5-dioxo-2,5-dihydro-1H-pyrrol-3-yl)amino)benzonitrile (68).

Compound **68** was isolated as a yellow solid in 53% yield. ^{1}H NMR (400 MHz, DMSO-d_6) δ 10.80 (s, 1H), 9.70 (s, 1H), 7.55 – 7.46 (m, 3H), 7.45 – 7.27 (m, 6H), 7.25 – 7.14 (m, 4H), 6.75 (dd, *J* = 21.2, 1.3 Hz, 2H), 5.24 (s, 2H), 3.19 (s, 3H). ^{13}C NMR (126 MHz, DMSO-d_6) δ 172.48, 169.01, 156.57, 152.94, 151.00, 145.73 (d, *J* = 10.9 Hz), 140.29, 138.80, 137.70, 136.56, 133.47 (d, *J* = 6.7 Hz), 130.55, 128.58, 128.52, 128.06, 127.74, 126.02, 125.23, 122.91, 122.86 (d, *J* = 2.8 Hz), 118.35, 118.07, 117.99, 115.68, 114.45 (d, *J* = 18.9 Hz), 110.00, 107.79, 100.35, 70.28, 54.59. HRMS (ES): calcd for $C_{31}H_{22}FN_3O_4$ $[M+H]^+$: 520.1673. Found: 520.1672.

3-((4-(4'-(benzyloxy)-3'-fluoro-4-methoxy-[1,1'-biphenyl]-3-yl)-2,5-dioxo-2,5-dihydro-1H-pyrrol-3-yl)amino)benzonitrile (69).

Compound **69** was isolated as a yellow solid in 62% yield. ^{1}H NMR (500 MHz, DMSO-d_6) δ 10.83 (s, 1H), 9.73 (s, 1H), 7.48 (d, *J* = 7.5 Hz, 4H), 7.41 (dd, *J* = 13.6, 5.9 Hz, 3H), 7.38 – 7.28 (m, 3H), 7.25 – 7.15 (m, 3H), 6.85 (s, 1H), 6.63 – 6.58 (m, 1H), 5.22 (s, 2H), 3.17 (s, 3H). ^{13}C NMR (126 MHz, DMSO-d_6) δ 172.47, 168.98, 155.78, 153.02, 151.08, 145.06 (d, *J* = 10.6 Hz), 138.75, 136.60, 133.44 (d, *J* = 6.5 Hz), 130.47, 128.62, 128.50, 128.40, 128.05, 127.79, 127.56, 126.14, 125.46, 123.39, 122.24 (d, *J* = 2.8 Hz), 119.57, 118.09, 115.85, 114.02, 113.87, 110.31, 110.09, 100.42, 70.34, 54.70. HRMS (ES): calcd for $C_{31}H_{22}FN_3O_4$ $[M+H]^+$: 520.1673. Found: 520.1672.

3-((4-(4-(2,3-dihydrobenzo[b][1,4]dioxin-5-yl)-2-methoxyphenyl)-2,5-dioxo-2,5-dihydro-1H-pyrrol-3-yl)amino)benzonitrile (70).

Compound **70** was isolated as a yellow solid in 47% yield. ^{1}H NMR (400 MHz, DMSO-d_6) δ 10.79 (s, 1H), 9.69 (s, 1H), 7.30 – 7.24 (m, 2H), 7.22 – 7.15 (m, 2H), 7.04 (dd, *J* = 7.9, 1.5 Hz, 1H), 6.89 – 6.81 (m, 3H), 6.78 (s, 1H), 6.58 (d, *J* = 1.3 Hz, 1H), 4.24 (dd, *J* = 14.2, 5.0 Hz, 4H), 3.12 (s, 3H). ^{13}C NMR (126 MHz, DMSO-d_6) δ 172.54, 169.07, 155.68, 143.72, 140.65, 138.85, 138.80, 137.78, 130.13, 129.65, 128.58, 126.03, 125.32, 123.00, 122.12, 120.85, 120.72, 118.14, 117.98, 116.44, 110.69, 110.12, 100.48, 64.01, 63.83, 54.43. HRMS (ES): calcd for $C_{26}H_{19}N_3O_5$ $[M+H]^+$: 454.1403. Found: 454.1381.

3-((4-(5-(2,3-dihydrobenzo[b][1,4]dioxin-5-yl)-2-methoxyphenyl)-2,5-dioxo-2,5-dihydro-1H-pyrrol-3-yl)amino)benzonitrile (71).

Compound **71** was isolated as a yellow solid in 58% yield. ^{1}H NMR (400 MHz, DMSO-d_6) δ 10.77 (s, 1H), 9.68 (s, 1H), 7.35 (dd, *J* = 8.6, 2.3 Hz, 1H), 7.31 (d, *J* = 2.3 Hz, 1H), 7.27 – 7.22 (m, 1H), 7.21 – 7.15 (m, 2H), 6.88 – 6.78 (m, 4H), 6.59 (d, *J* = 8.7 Hz, 1H), 4.24 (dd, *J* = 15.7, 5.0 Hz, 4H), 3.21 (s, 3H). ^{13}C NMR (126 MHz, DMSO-d_6) δ 172.48, 169.01, 155.36, 143.71, 140.56, 138.78, 138.04, 131.01, 130.48, 129.69, 128.84, 128.59,

126.17, 125.47, 123.28, 122.09, 120.68, 118.72, 118.11, 115.93, 110.17, 109.43, 100.73, 64.08, 63.81, 54.66. HRMS (ES): calcd for $C_{26}H_{19}N_3O_5$ [M+H]+: 454.1403. Found: 454.1412.

3-((2,5-dioxo-4-(3,3',4',5'-tetramethoxy-[1,1'-biphenyl]-4-yl)-2,5-dihydro-1H-pyrrol-3-yl)amino)benzonitrile (72).

Compound **72** was isolated as a yellow solid in 19% yield. ^{1}H NMR (500 MHz, DMSO-d_6) δ 10.82 (s, 1H), 9.72 (s, 1H), 7.32 (d, *J* = 7.9 Hz, 1H), 7.26 – 7.18 (m, 4H), 6.83 (s, 2H), 6.71 (d, *J* = 8.5 Hz, 2H), 3.84 (s, 6H), 3.69 (s, 3H), 3.20 (s, 3H). ^{13}C NMR (126 MHz, DMSO-d_6) δ 172.49, 169.02, 156.42, 153.03, 142.35, 138.75, 137.76, 137.29, 136.24, 130.38, 128.63, 126.09, 125.39, 122.87, 118.65, 118.31, 118.15, 109.99, 108.36, 104.65, 100.50, 60.05, 55.93, 54.62. HRMS (ES): calcd for $C_{27}H_{23}N_3O_6$ $[M+H]^+$: 486.1665. Found: 486.1682.

3-((2,5-dioxo-4-(3',4,4',5'-tetramethoxy-[1,1'-biphenyl]-3-yl)-2,5-dihydro-1H-pyrrol-3-yl)amino)benzonitrile (73).

Compound **73** was isolated as a yellow solid in 23% yield. ^{1}H NMR (400 MHz, DMSO-d_6) δ 10.80 (s, 1H), 9.71 (s, 1H), 7.51 – 7.45 (m, 1H), 7.43 (d, *J* = 2.4 Hz, 1H), 7.27 – 7.18 (m, 3H), 6.85 (s, 1H), 6.75 (s, 2H), 6.63 (d, *J* = 8.7 Hz, 1H), 3.84 (s, 6H), 3.68 (s, 3H), 3.23 (s, 3H). ^{13}C NMR (126 MHz, DMSO-d_6) δ 172.41, 168.99, 155.74, 153.05, 138.71, 138.19, 136.72, 135.95, 132.43, 128.84, 128.66, 128.05, 126.19, 125.57, 123.53, 119.41, 118.13, 110.17, 110.10, 104.16, 100.71, 60.06, 55.91, 54.76. HRMS (ES): calcd for $C_{27}H_{23}N_3O_6$ $[M+H]^+$: 486.1665. Found: 486.1682.

3-((4-(2-methoxy-4-(thiophen-3-yl)phenyl)-2,5-dioxo-2,5-dihydro-1H-pyrrol-3-yl)amino)benzonitrile (74).

Compound **74** was isolated as a yellow solid in 45% yield. ^{1}H NMR (500 MHz, DMSO-d_6) δ 10.80 (s, 1H), 9.68 (s, 1H), 7.84 (dd, *J* = 2.9, 1.3 Hz, 1H), 7.61 (dd, *J* = 5.0, 2.9 Hz, 1H), 7.52 (dd, *J* = 5.0, 1.2 Hz, 1H), 7.30 (s, 2H), 7.22 (dt, *J* = 7.3, 1.4 Hz, 1H), 7.18 – 7.10 (m, 2H), 6.89 (s, 1H), 6.83 (s, 1H), 3.20 (s, 3H). ^{13}C NMR (126 MHz, DMSO-d_6) δ 172.54, 169.07, 156.60, 141.38, 138.90, 137.56, 136.63, 130.58, 128.60, 126.84, 126.47, 125.96, 124.99, 123.00, 121.40, 118.14, 118.06, 117.76, 110.13, 107.44, 100.65, 54.59. HRMS (ES): calcd for $C_{22}H_{15}N_3O_3S$ $[M+H]^+$: 402.0912. Found: 402.0901.

3-((4-(2-methoxy-5-(thiophen-3-yl)phenyl)-2,5-dioxo-2,5-dihydro-1H-pyrrol-3-yl)amino)benzonitrile (75).

Compound **75** was isolated as a yellow solid in 61% yield. ^{1}H NMR (500 MHz, DMSO-d_6) δ 10.82 (s, 1H), 9.72 (s, 1H), 7.64 (dd, *J* = 2.9, 1.3 Hz, 1H), 7.60 (dd, *J* = 5.0, 2.9 Hz, 1H), 7.55 (dd, *J* = 6.9, 2.3 Hz, 2H), 7.42 (dd, *J* = 5.0, 1.3 Hz, 1H), 7.23 (dt, *J* = 7.3, 1.5 Hz, 1H), 7.13 (tt, *J* = 4.8, 3.6 Hz, 2H), 6.91 (t, *J* = 1.5 Hz, 1H), 6.62 – 6.57 (m, 1H), 3.17 (s, 3H). ^{13}C NMR (126 MHz, DMSO-d_6) δ 172.50, 169.00, 155.52, 141.11, 138.87, 138.00,

128.63, 128.13, 127.39, 127.24, 126.79, 126.19, 126.13, 125.27, 123.35, 119.51, 119.44, 118.15, 110.25, 110.17, 100.42, 54.65. HRMS (ES): calcd for $C_{22}H_{15}N_3O_3S$ $[M+H]^+$: 402.0912. Found: 402.0902.

3-((4-(2-methoxy-4-(pyridin-3-yl)phenyl)-2,5-dioxo-2,5-dihydro-1H-pyrrol-3-yl)amino)benzonitrile (76).

Compound **76** was isolated as a yellow solid in 11% yield. ^{1}H NMR (500 MHz, Acetone-d_6) δ 9.68 (s, 1H), 8.85 (d, *J* = 2.1 Hz, 1H), 8.76 (s, 1H), 8.57 (dd, *J* = 4.8, 1.5 Hz, 1H), 8.03 – 7.97 (m, 1H), 7.54 (d, *J* = 7.9 Hz, 1H), 7.44 (dd, *J* = 7.9, 4.8 Hz, 1H), 7.33 – 7.23 (m, 4H), 6.97 (s, 1H), 6.86 (d, *J* = 1.5 Hz, 1H), 3.35 (s, 3H). ^{13}C NMR (126 MHz, Acetone-d_6) δ 172.51, 169.36, 158.18, 149.58, 149.18, 140.66, 139.97, 138.65, 137.18, 135.12, 132.04, 129.72, 127.27, 126.05, 124.38, 124.24, 120.34, 119.71, 118.68, 112.21, 109.41, 101.91, 55.25. HRMS (ES): calcd for $C_{23}H_{16}N_4O_3$ $[M+H]^+$: 397.1301. Found: 397.1293.

3-((4-(2-methoxy-5-(pyridin-3-yl)phenyl)-2,5-dioxo-2,5-dihydro-1H-pyrrol-3-yl)amino)benzonitrile (77).

Compound **77** was isolated as a yellow solid in 27% yield. ^{1}H NMR (500 MHz, DMSO-d_6) δ 10.80 (s, 1H), 9.77 (s, 1H), 8.78 (d, *J* = 1.9 Hz, 1H), 8.52 (dd, *J* = 4.7, 1.5 Hz, 1H), 7.99 – 7.92 (m, 1H), 7.56 (dt, *J* = 6.9, 2.3 Hz, 2H), 7.46 (dd, *J* = 7.9, 4.8 Hz, 1H), 7.26 – 7.19 (m, 3H), 6.85 (s, 1H), 6.67 (d, *J* = 8.5 Hz, 1H), 3.21 (s, 3H). ^{13}C NMR (126 MHz, DMSO-d_6) δ 172.52, 169.02, 156.37, 147.83, 147.42, 138.76, 138.35, 135.33, 133.73, 128.88, 128.79, 128.68, 128.09, 126.20, 125.63, 123.77, 123.51, 119.95, 118.10, 110.59, 110.06, 100.14, 54.80. HRMS (ES): calcd for $C_{23}H_{16}N_4O_3$ $[M+H]^+$: 397.1301. Found: 397.1294.

3-((4-(4-(2,6-dichloropyridin-3-yl)-2-methoxyphenyl)-2,5-dioxo-2,5-dihydro-1H-pyrrol-3-yl)amino)benzonitrile (78).

Compound **78** was isolated as a yellow solid in 60% yield. ^{1}H NMR (500 MHz, DMSO-d_6) δ 10.85 (s, 1H), 9.79 (s, 1H), 7.88 (d, *J* = 8.0 Hz, 1H), 7.69 (d, *J* = 8.0 Hz, 1H), 7.39 (d, *J* = 7.8 Hz, 1H), 7.29 – 7.18 (m, 3H), 7.06 (dd, *J* = 7.8, 1.4 Hz, 1H), 6.84 (s, 1H), 6.65 (d, *J* = 1.1 Hz, 1H), 3.14 (s, 3H). ^{13}C NMR (126 MHz, DMSO-d_6) δ 172.40, 168.90, 155.95, 147.75, 147.29, 143.04, 138.79, 138.26, 136.99, 135.37, 130.25, 128.71, 126.30, 125.51, 123.69, 123.24, 120.65, 119.68, 118.26, 110.78, 110.09, 99.69, 54.71. HRMS (ES): calcd for $C_{23}H_{14}Cl_2N_4O_3$ $[M+H]^+$: 465.0521. Found: 465.0499.

N-(4-(4-((3-cyanophenyl)amino)-2,5-dioxo-2,5-dihydro-1H-pyrrol-3-yl)-3-methoxyphenyl)isobutyramide (79).

Compound **79** was isolated as a yellow solid in 41% yield. ^{1}H NMR (500 MHz, DMSO-d_6) δ 10.75 (s, 1H), 9.84 (s, 1H), 9.58 (s, 1H), 7.24 (d, *J* = 7.6 Hz, 1H), 7.21 – 7.13 (m, 3H), 7.09 (dd, *J* = 8.3, 1.0 Hz, 1H), 7.03 (s, 1H), 6.83 (s, 1H), 3.06 (s, 3H), 2.57 (quint, 1H), 1.08 (s, 3H), 1.07 (s, 3H). ^{13}C NMR (126 MHz, DMSO-d_6) δ 175.29,

172.70, 169.23, 156.45, 141.11, 139.07, 136.80, 130.26, 128.59, 125.72, 124.69, 122.56, 118.17, 113.60, 110.27, 110.16, 101.07, 100.43, 54.16, 34.97, 19.45. HRMS (ES): calcd for $C_{22}H_{20}N_4O_4$ $[M+H]^+$: 405.1563. Found: 405.1574.

N-(3-(4-((3-cyanophenyl)amino)-2,5-dioxo-2,5-dihydro-1H-pyrrol-3-yl)-4-methoxyphenyl)isobutyramide (80).

Compound **80** was isolated as a yellow solid in 48% yield. ^{1}H NMR (500 MHz, DMSO-d_6) δ 10.80 (s, 1H), 9.70 (s, 1H), 9.66 (s, 1H), 7.56 – 7.52 (m, 2H), 7.24 (d, *J* = 7.7 Hz, 1H), 7.14 (t, *J* = 7.9 Hz, 1H), 7.03 (dd, *J* = 8.2, 1.2 Hz, 1H), 6.91 – 6.88 (m, 1H), 6.46 (d, *J* = 9.0 Hz, 1H), 3.08 (s, 3H), 2.57 (quint, 1H), 1.09 (s, 3H), 1.08 (s, 3H). ^{13}C NMR (126 MHz, DMSO-d_6) δ 174.64, 172.45, 168.97, 152.05, 138.87, 137.84, 132.12, 128.55, 125.99, 124.96, 123.23, 120.99, 120.38, 118.82, 118.21, 110.14, 109.71, 100.38, 54.48, 34.78, 19.58. HRMS (ES): calcd for $C_{22}H_{20}N_4O_4$ $[M+H]^+$: 405.1563. Found: 405.1573.

3-((4-(4-bromo-2-methoxyphenyl)-2,5-dioxo-2,5-dihydro-1H-pyrrol-3-yl)amino)benzonitrile (81).

Compound **81** was isolated as a yellow solid in 71% yield. ^{1}H NMR (400 MHz, DMSO-d_6) δ 10.84 (s, 1H), 9.75 (s, 1H), 7.30 (d, *J* = 7.6 Hz, 1H), 7.25 – 7.19 (m, 2H), 7.18 – 7.11 (m, 2H), 6.83 (s, 1H), 6.73 (d, *J* = 1.7 Hz, 1H), 3.13 (s, 3H). ^{13}C NMR (126 MHz, DMSO-d_6) δ 172.25, 168.83, 156.92, 138.80, 138.12, 131.63, 128.74, 126.35, 125.39, 123.19, 122.77, 122.26, 118.64, 118.03, 113.07, 110.16, 99.33, 55.03. HRMS (ES): calcd for $C_{18}H_{12}BrN_3O_3$ $[M+H]^+$: 398.0140. Found: 398.0157.

3-((4-(5-bromo-2-methoxyphenyl)-2,5-dioxo-2,5-dihydro-1H-pyrrol-3-yl)amino)benzonitrile (82).

Compound **82** was isolated as a yellow solid in 32% yield. ^{1}H NMR (400 MHz, DMSO-d_6) δ 10.85 (s, 1H), 9.79 (s, 1H), 7.41 (d, *J* = 2.5 Hz, 1H), 7.37 (dd, *J* = 8.8, 2.6 Hz, 1H), 7.28 (dt, *J* = 7.5, 1.2 Hz, 1H), 7.21 (t, *J* = 7.8 Hz, 1H), 7.16 – 7.11 (m, 1H), 6.89 (t, *J* = 1.7 Hz, 1H), 6.50 (d, *J* = 8.9 Hz, 1H), 3.11 (s, 3H). ^{13}C NMR (126 MHz, DMSO-d_6) δ 172.27, 168.73, 155.51, 138.76, 138.52, 132.34, 131.83, 128.73, 126.42, 125.52, 123.53, 121.41, 118.09, 111.95, 111.17, 110.19, 98.76, 54.82. HRMS (ES): calcd for $C_{18}H_{12}BrN_3O_3$ $[M+H]^+$: 398.0140. Found: 398.0147.

Associated Content

Supporting Information

Supplementary NanoBRET figures, data collection and refinement statistics for the two crystal structures, table of NanoBRET assay conditions used for the cellular cross-screening, analytical chemistry methods, characterization data for intermediate compounds, raw NMR traces and HPLC chromatograms for lead compounds.

Combined table of all *in vitro* assay data.

In vitro cross-screening data.

SMILES strings for the compounds.

Accession Codes

The atomic coordinates for SLK:**55** and STK10:**56** are available from the Protein Data Bank with ID numbers 6HVD and 6HXF respectively.

Author Information

Corresponding author

Jonathan M. Elkins - Centre for Medicines Discovery, University of Oxford, Old Road Campus Research Building, Old Road Campus, Roosevelt Drive, Oxford, OX3 7DQ, UK; Structural Genomics Consortium, University of Campinas (UNICAMP), Av. Dr. André Tosello, 550, Barão Geraldo, Campinas / SP 13083-886, Brazil; Email: jon.elkins@cmd.ox.ac.uk

William J. Zuercher - Structural Genomics Consortium, UNC Eshelman School of Pharmacy, University of North Carolina at Chapel Hill, Chapel Hill, NC 27599, USA; Email: william.zuercher@unc.edu

Authors

Ricardo A. M. Serafim - Center for Medicinal Chemistry (CQMED), Center for Molecular Biology and Genetic Engineering (CBMEG), University of Campinas (UNICAMP), Campinas, SP 13083-875, Brazil; Structural Genomics Consortium, University of Campinas (UNICAMP), Av. Dr. André Tosello, 550, Barão Geraldo, Campinas / SP 13083-886, Brazil.

Fiona J. Sorrell - Centre for Medicines Discovery, University of Oxford, Old Road Campus Research Building, Old Road Campus, Roosevelt Drive, Oxford, OX3 7DQ, UK.

Benedict-Tilman Berger - Structural Genomics Consortium, Johann Wolfgang Goethe University, Buchmann Institute for Molecular Life Sciences, Max-von-Laue-Str. 15, D-60438 Frankfurt am Main, DE, Germany; Institute for Pharmaceutical Chemistry, Johann Wolfgang Goethe University, Max-von-Laue-Str. 9, D-60438 Frankfurt am Main, DE, Germany.

Ross J. Collins - Medicines Discovery Institute, School of Biosciences, Cardiff University, Cardiff, CF10 3AT, UK.

Stanley N. S. Vasconcelos - Center for Medicinal Chemistry (CQMED), Center for Molecular Biology and Genetic Engineering (CBMEG), University of Campinas (UNICAMP), Campinas, SP 13083-875, Brazil; Structural Genomics Consortium, University of Campinas (UNICAMP), Av. Dr. André Tosello, 550, Barão Geraldo, Campinas / SP 13083-886, Brazil.

Katlin B. Massirer - Center for Medicinal Chemistry (CQMED), Center for Molecular Biology and Genetic Engineering (CBMEG), University of Campinas (UNICAMP), Campinas, SP 13083-875, Brazil; Structural Genomics Consortium, University of Campinas (UNICAMP), Av. Dr. André Tosello, 550, Barão Geraldo, Campinas / SP 13083-886, Brazil.

Stefan Knapp - Structural Genomics Consortium, Johann Wolfgang Goethe University, Buchmann Institute for Molecular Life Sciences, Max-von-Laue-Str. 15, D-60438 Frankfurt am Main, DE, Germany; Institute for Pharmaceutical Chemistry, Johann Wolfgang Goethe University, Max-von-Laue-Str. 9, D-60438 Frankfurt am Main, DE, Germany.

James Bennett - Centre for Medicines Discovery, University of Oxford, Old Road Campus Research Building, Old Road Campus, Roosevelt Drive, Oxford, OX3 7DQ, UK.

Oleg Fedorov - Centre for Medicines Discovery, University of Oxford, Old Road Campus Research Building, Old Road Campus, Roosevelt Drive, Oxford, OX3 7DQ, UK.

Hitesh Patel - Medicines Discovery Institute, School of Biosciences, Cardiff University, Cardiff, CF10 3AT, UK.

Notes

The authors declare no competing interests.

Acknowledgements

We thank Kamal R. Abdul Azeez for assistance with NanoBRET measurements. We thank the NMR facility of the Department of Pharmaceutical/Medicinal Chemistry of the University of Tübingen for assistance.
The SGC is a registered charity (number 1097737) that receives funds from AbbVie, Bayer Pharma AG, Boehringer Ingelheim, Canada Foundation for Innovation, Eshelman Institute for Innovation, Genome

Canada, the EU/EFPIA/OICR/McGill/KTH/Diamond Innovative Medicines Initiative 2 Joint Undertaking (EUbOPEN grant n° 875510), Janssen, Merck KGaA Darmstadt Germany, MSD, Novartis Pharma AG, Ontario Ministry of Economic Development and Innovation, Pfizer, São Paulo Research Foundation-FAPESP, Takeda, and Wellcome [106169/ZZ14/Z].

R.A.M.S. and S.N.S.V. received FAPESP fellowships (2016/25320-6 and 2018/09475-5, respectively).

Abbreviations Used

ERM, ezrin/radixin/moesin; SLK, STE20-like kinase; STK10, serine/threonine kinase 10; S(35), (number of non-mutant kinases with %Ctrl <35)/(number of non-mutant kinases tested).

References

(1) Belkina, N. V; Liu, Y.; Hao, J.-J.; Karasuyama, H.; Shaw, S. LOK Is a Major ERM Kinase in Resting Lymphocytes and Regulates Cytoskeletal Rearrangement through ERM Phosphorylation. *PNAS* **2009**, *106* (12), 4707–4712.

(2) Hipfner, D. R.; Keller, N.; Cohen, S. M. Slik Sterile-20 Kinase Regulates Moesin Activity to Promote Epithelial Integrity during Tissue Growth. *Genes Dev.* **2004**, *18* (18), 2243–2248.

(3) Pearson, M. A.; Reczek, D.; Bretscher, A.; Karplus, P. A. Structure of the ERM Protein Moesin Reveals the FERM Domain Fold Masked by an Extended Actin Binding Tail Domain. *Cell* **2000**, *101* (3), 259–270.

(4) Gary, R.; Bretscher, A. Ezrin Self-Association Involves Binding of an N-Terminal Domain to a Normally Masked C-Terminal Domain That Includes the F-Actin Binding Site. *Mol. Biol. Cell* **1995**, *6* (8), 1061–1075.

(5) Bretscher, A. Regulation of Cortical Structure by the Ezrin-Radixin-Moesin Protein Family. *Curr. Opin. Cell Biol.* **1999**, *11* (1), 109–116.

(6) Viswanatha, R.; Ohouo, P. Y.; Smolka, M. B.; Bretscher, A. Local Phosphocycling Mediated by LOK/SLK Restricts Ezrin Function to the Apical Aspect of Epithelial Cells. *J. Cell Biol.* **2012**, *199* (6), 969–984.

(7) Kuramochi, S.; Moriguchi, T.; Kuida, K.; Endo, J.; Semba, K.; Nishida, E.; Karasuyama, H. LOK Is a Novel Mouse STE20-like Protein Kinase That Is Expressed Predominantly in Lymphocytes. *J. Biol. Chem.* **1997**, *272* (36), 22679–22684.

(8) Sabourin, L. A.; Rudnicki, M. A. Induction of Apoptosis by SLK, a Ste20-Related Kinase. *Oncogene* **1999**, *18* (52), 7566–7575.

(9) Yamada, E.; Tsujikawa, K.; Itoh, S.; Kameda, Y.; Kohama, Y.; Yamamoto, H. Molecular Cloning and Characterization of a Novel Human STE20-like Kinase, HSLK. *Biochim. Biophys. Acta* **2000**, *1495* (3), 250–262.

(10) Walter, S. A.; Cutler, R. E.; Martinez, R.; Gishizky, M.; Hill, R. J. Stk10, a New Member of the Polo-like Kinase Kinase Family Highly Expressed in Hematopoietic Tissue. *J. Biol. Chem.* **2003**, *278* (20), 18221–18228.

(11) Ellinger-Ziegelbauer, H.; Karasuyama, H.; Yamada, E.; Tsujikawa, K.; Todokoro, K.; Nishida, E. Ste20-like Kinase (SLK), a Regulatory Kinase for Polo-like Kinase (Plk) during the G2/M Transition in Somatic Cells. *Genes to cells* **2000**, *5* (6), 491–498.

(12) Johnson, T. M.; Antrobus, R.; Johnson, L. N. Plk1 Activation by Ste20-like Kinase (Slk) Phosphorylation and Polo-Box Phosphopeptide Binding Assayed with the Substrate Translationally Controlled Tumor Protein (TCTP). *Biochemistry* **2008**, *47* (12), 3688–3696.

(13) Li, J.; Wang, R.; Gannon, O. J.; Rezey, A. C.; Jiang, S.; Gerlach, B. D.; Liao, G.; Tang, D. D. Polo-like Kinase 1 Regulates Vimentin Phosphorylation at Ser-56 and Contraction in Smooth Muscle. *J. Biol. Chem.* **2016**, *291* (45), 23693–23703.

(14) Leroy, C.; Belkina, N. V.; Long, T.; Deruy, E.; Dissous, C.; Shaw, S.; Tulasne, D. Caspase

Cleavages of the Lymphocyte-Oriented Kinase Prevent Ezrin, Radixin, and Moesin Phosphorylation during Apoptosis. *J. Biol. Chem.* **2016**, *291* (19), 10148–10161.

(15) Pelaseyed, T.; Sauvanet, C.; Viswanatha, R.; Filter, J. J.; Goldberg, M. L.; Bretscher, A. Ezrin Activation by LOK Phosphorylation Involves a PIP2-Dependent Wedge Mechanism. *Elife* **2017**, *6*, 1–18.

(16) Sabourin, L. A.; Tamai, K.; Seale, P.; Wagner, J.; Rudnicki, M. A. Caspase 3 Cleavage of the Ste20-Related Kinase SLK Releases and Activates an Apoptosis-Inducing Kinase Domain and an Actin-Disassembling Region. *Mol. Cell. Biol.* **2000**, *20* (8), 2949–2949.

(17) Pike, A. C. W.; Rellos, P.; Niesen, F. H.; Turnbull, A.; Oliver, A. W.; Parker, S. a; Turk, B. E.; Pearl, L. H.; Knapp, S. Activation Segment Dimerization: A Mechanism for Kinase Autophosphorylation of Non-Consensus Sites. *EMBO J.* **2008**, *27* (4), 704–714.

(18) Delarosa, S.; Guillemette, J.; Papillon, J.; Han, Y.-S.; Kristof, A. S.; Cybulsky, A. V. Activity of the Ste20-like Kinase, SLK, Is Enhanced by Homodimerization. *Am. J. Physiol. Renal Physiol.* **2011**, *301* (3), F554-64.

(19) Elkins, J. M.; Fedele, V.; Szklarz, M.; Abdul Azeez, K. R.; Salah, E.; Mikolajczyk, J.; Romanov, S.; Sepetov, N.; Huang, X.-P.; Roth, B. L.; Al Haj Zen, A.; Fourches, D.; Muratov, E.; Tropsha, A.; Morris, J.; Teicher, B. A.; Kunkel, M.; Polley, E.; Lackey, K. E.; Atkinson, F. L.; Overington, J. P.; Bamborough, P.; Müller, S.; Price, D. J.; Willson, T. M.; Drewry, D. H.; Knapp, S.; Zuercher, W. J. Comprehensive Characterization of the Published Kinase Inhibitor Set. *Nat. Biotechnol.* **2016**, *34* (1), 95–103.

(20) Drewry, D. H.; Wells, C. I.; Andrews, D. M.; Angell, R.; Al-Ali, H.; Axtman, A. D.; Capuzzi, S. J.; Elkins, J. M.; Ettmayer, P.; Frederiksen, M.; Gileadi, O.; Gray, N.; Hooper, A.; Knapp, S.; Laufer, S.; Luecking, U.; Michaelides, M.; Müller, S.; Muratov, E.; Denny, R. A.; Saikatendu, K. S.; Treiber, D. K.; Zuercher, W. J.; Willson, T. M. Progress towards a Public Chemogenomic Set for Protein Kinases and a Call for Contributions. *PLoS One* **2017**, *12* (8), e0181585.

(21) Roovers, K.; Wagner, S.; Storbeck, C. J.; O'Reilly, P.; Lo, V.; Northey, J. J.; Chmielecki, J.; Muller, W. J.; Siegel, P. M.; Sabourin, L. A. The Ste20-like Kinase SLK Is Required for ErbB2-Driven Breast Cancer Cell Motility. *Oncogene* **2009**, *28* (31), 2839–2848.

(22) GAO, Y.; HA, Y.-S.; KWON, T. G.; CHO, Y.-C.; LEE, S.; LEE, J. N. Characterization of Kinase Expression Related to Increased Migration of PC-3M Cells Using Global Comparative Phosphoproteome Analysis. *Cancer Genomics - Proteomics* **2020**, *17* (5), 543–553.

(23) Cybulsky, A. V.; Guillemette, J.; Papillon, J.; Abouelazm, N. T. Regulation of Ste20-like Kinase, SLK, Activity: Dimerization and Activation Segment Phosphorylation. *PLoS One* **2017**, *12* (5), e0177226.

(24) Wagner, S.; Storbeck, C. J.; Roovers, K.; Chaar, Z. Y.; Kolodziej, P.; McKay, M.; Sabourin, L. A. FAK/Src-Family Dependent Activation of the Ste20-Like Kinase SLK Is Required for Microtubule-Dependent Focal Adhesion Turnover and Cell Migration. *PLoS One* **2008**, *3* (4), e1868.

(25) Doble, B. W.; Woodgett, J. R. GSK-3: Tricks of the Trade for a Multi-Tasking Kinase. *J. Cell Sci.* **2003**, *116* (Pt 7), 1175–1186.

(26) Kabsch, W. XDS. *Acta crystallogr.* **2010**, *D66* (Pt 2), 125–132.

(27) Evans, P. R. An Introduction to Data Reduction: Space-Group Determination, Scaling and Intensity Statistics. *Acta crystallogr.* **2011**, *D67* (Pt 4), 282–292.

(28) McCoy, A. J.; Grosse-Kunstleve, R. W.; Adams, P. D.; Winn, M. D.; Storoni, L. C.; Read, R. J. Phaser Crystallographic Software. *J. Appl. Cryst.* **2007**, *40* (Pt 4), 658–674.

(29) Murshudov, G. N.; Skubák, P.; Lebedev, A. A.; Pannu, N. S.; Steiner, R. A.; Nicholls, R. A.; Winn, M. D.; Long, F.; Vagin, A. A. REFMAC5 for the Refinement of Macromolecular Crystal Structures. *Acta crystallogr.* **2011**, *D67* (Pt 4), 355–367.

(30) Adams, P. D.; Afonine, P. V; Bunkóczi, G.; Chen, V. B.; Davis, I. W.; Echols, N.; Headd, J. J.; Hung, L.-W.; Kapral, G. J.; Grosse-Kunstleve, R. W.; McCoy, A. J.; Moriarty, N. W.; Oeffner, R.; Read, R. J.; Richardson, D. C.; Richardson, J. S.; Terwilliger, T. C.; Zwart, P. H. PHENIX : A Comprehensive Python-Based System for Macromolecular Structure Solution. *Acta Crystallogr. Sect. D Biol. Crystallogr.* **2010**, *66* (2), 213–221.

(31) Emsley, P.; Lohkamp, B.; Scott, W. G.; Cowtan, K. Features and Development of Coot. *Acta crystallogr.* **2010**, *D66* (Pt 4), 486–501.

(32) Lee, C. F. F.; Holownia, A.; Bennett, J. M.; Elkins, J. M.; St. Denis, J. D.; Adachi, S.; Yudin, A. K. Oxalyl Boronates Enable Modular Synthesis of Bioactive Imidazoles. *Angew. Chemie Int. Ed.* **2017**, *56* (22), 6264–6267.

Table of Contents Graphic

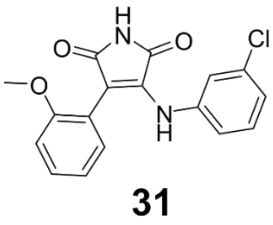

31